Chem Soc Rev

REVIEW ARTICLE

View Article Online
View Journal | View Issue

Cite this: *Chem. Soc. Rev.*, 2021, **50**, 589

Revisiting imidazolium receptors for the recognition of anions: highlighted research during 2010–2019

Ying Hu, †[ab] Shuangshuang Long, †[cd] Haiyan Fu,[e] Yuanbin She, *[a] Zhaochao Xu *[c] and Juyoung Yoon *[b]

Imidazolium based receptors selectively recognize anions, and have received more and more attention. In 2006 and 2010, we reviewed the mechanism and progress of imidazolium salt recognition of anions, respectively. In the past ten years, new developments have emerged in this area, including some new imidazolium motifs and the identification of a wider variety of biological anions. In this review, we discuss the progress of imidazolium receptors for the recognition of anions in the period of 2010–2019 and highlight the trends in this area. We first classify receptors based on motifs, including some newly emerging receptors, as well as new advances in existing receptor types at this stage. Then we discuss separately according to the types of anions, including ATP, GTP, DNA and RNA.

Received 1st June 2020

DOI: 10.1039/d0cs00642d

rsc.li/chem-soc-rev

1. Introduction

Studies of anion selective receptors in the context of biological and medical applications have been numerous during the past twenty years. However, challenges still exist in developing receptors that selectively bind anions in water.[1] Nevertheless, significant advances have been made in developing new types of anion receptors in recent years.[2–8] Imidazolium groups have been used as the basis of the new receptors because they strongly interact with anions through $(C–H)^{+}\cdots X^{-}$ type ionic hydrogen bonds and charge–charge electrostatic interactions.[2] An advantageous feature of imidazolium receptors is that they display high affinities for anions in aqueous solutions, and, in

[a] *College of Chemical Engineering, Zhejiang University of Technology, Hangzhou, Zhejiang 310014, China. E-mail: sheyb@zjut.edu.cn*
[b] *Department of Chemistry and Nanoscience, Ewha Womans University, Seoul 120-750, Korea. E-mail: jyoon@ewha.ac.kr*
[c] *Key Laboratory of Separation Science for Analytical Chemistry, Dalian Institute of Chemical Physics, Chinese Academy of Sciences, Dalian 116023, China. E-mail: zcxu@dicp.ac.cn*
[d] *School of Chemistry and Chemical Engineering, University of South China, Hengyang 421001, China*
[e] *The Modernization Engineering Technology Research Center of Ethnic Minority Medicine of Hubei Province, School of Pharmaceutical Sciences, South-Central University for Nationalities, Wuhan 430074, China*
† These two authors contributed equally.

Ying Hu

Ying Hu received her Bachelor's degree from East China University of Science and Technology (Shanghai, 2011) and PhD degree under the supervision of Prof. Juyoung Yoon in the Department of Chemistry and Nano Science at Ewha Womans University (South Korea, 2017). She is currently part of Prof. Yuanbin She's research group at Zhejiang University of Technology (Hangzhou) as a lecturer. Her research interests include fluorescent chemosensors and molecular recognition.

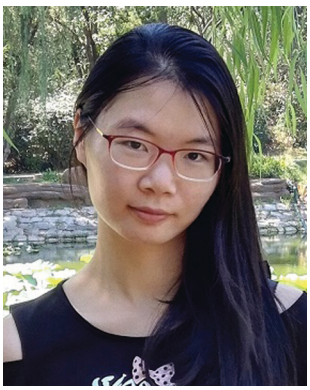

Shuangshuang Long

Shuangshuang Long was born in Hunan, China, in 1990. She got her BSc from Huazhong Agricultural University in June 2013. Her PhD studies were carried out at the Dalian Institute of Chemical Physics (DICP), Chinese Academy of Sciences, with Professor Zhaochao Xu (2013–2019). She joined the University of South China in September 2019. Her research interests are focused on fluorescent probes for protein phosphorylation.

some cases, in pure water.[3] Thus, among various types of anion receptors studied to date, those that utilize imidazolium ions have been extensively investigated. These efforts have led to the discovery of interesting anion sensor receptors that can be utilized as sensors for DNA,[4,5] RNA[6] and ATP.[7,8]

In previous tutorial reviews on imidazolium receptors,[2,3] we discussed the nature of $(C–H)^{+}\cdots X^{-}$ type ionic hydrogen bonding between various imidazolium structures and different anions. During the period 2010–2019, new and essential contributions have arisen from studies of imidazolium receptors, such as those related to the combination of imidazolium with halogen-bonding, the expansion of imidazolium conjugated systems, and the development of many new scaffolds. All these findings have given increased flexibility to the use of imidazolium receptors in the design of anion sensors for biological applications. In this review, we highlight developments made in the field of imidazolium receptors from 2010 to 2019. The presentation is not intended to provide a comprehensive overview of this area but rather a summary of advances in receptor structure, which is intended to help workers design and use imidazolium receptors in their research.

2. New imidazolium motifs and derivatives

2.1 Extended imidazolium conjugated systems

Imidazolium itself is not a chromophore. For the purpose of signaling binding to anions, the imidazolium group is usually

Haiyan Fu

Prof. Haiyan Fu is a member of the Academic Committee and the head of the Department of Pharmaceutical Analysis of South Central University for Nationalities. She received her PhD in analytical chemistry from Hunan University in 2010. Then she worked at the School of Pharmaceutical Sciences, South Central University for Nationalities, and became a full professor in 2017. Her research mainly focuses on the development and application of new methods for drug and food security through chemometrics combined with nanometer materials and spectroscopic techniques. Prof. Fu has over 120 publications, including in Biosens. Bioelectron., Carbon, Sensor Actuat. B: Chem., Anal. Chem., Food Chem., Anal. Chim. Acta., etc.

Yuanbin She

Prof. Yuanbin She is a professor of the College of Chemical Engineering at Zhejiang University of Technology (P. R. China). He received his PhD in engineering from Dalian University of Technology (P. R. China) in 1997. He then worked at Beijing University of Technology (P. R. China) until 2014 before moving to Zhejiang University of Technology. His research mainly focuses on the molecular design, synthesis and application of metalloporphyrins and biometic catalysis.

Zhaochao Xu

Prof. Zhaochao Xu was born in Qingdao, China, in 1979. He received his PhD in 2006 from Dalian University of Technology under the supervision of Prof. Xuhong Qian. Subsequently, he joined Prof. Juyoung Yoon's group at Ewha Womans University as a postdoctoral researcher. In October 2008, he became a Herchel Smith Research Fellow at University of Cambridge in Prof. David R. Spring's group. In 2011, he moved to Dalian Institute of Chemical Physics, CAS, where he is currently a Professor. His research is focusing on the development of fluorescent probes for the selective recognition and fluorescence imaging of biologically important species.

Juyoung Yoon

Prof. Juyoung Yoon received his PhD (1994) from The Ohio State University. After completing post-doctoral research at UCLA and at Scripps Research Institute, he joined the faculty at Silla University in 1998. In 2002, he moved to the Ewha Womans University, where he is currently a Distinguished Professor of the Department of Chemistry and Nano Science. His research interests include investigations of fluorescent probes, activatable photosensitizers, theranostics and organic functional materials. He is listed as a highly cited researcher in chemistry of 2014–2019 with an h-index of 101.

linked to an external chromophore to form a chemosensor, which translates the recognition event into an optical signal. Another approach is to fuse the imidazolium group with a conjugated system (Fig. 1a), thus producing an extended imidazolium π system that can act as both an anion receptor and a signal reporter.[9] From the perspective of synthesis, the usual strategies employed for this purpose are to link an aromatic system to the imidazolium ring across neighboring C4 and C5 positions (Fig. 1b) or to conjugate an aromatic ring with the imidazolium nitrogen atom (Fig. 1c).

Mahapatra and co-workers devised a ratiometric fluorescent chemosensor **1** based on a xanthine alkaloid theophylline moiety for the detection of dihydrogen phosphate (Fig. 1b).[10] This is the first example in which a theophylline moiety was used instead of a well-established imidazolium receptor as the central binding zone for anion sensing. Chemosensor **1** exhibited a naphthalene emission band at 343 nm in CH_3CN/H_2O (9 : 1) upon excitation at 288 nm. In the presence of $H_2PO_4^-$ anions, the naphthalene emission was significantly quenched, and a new broad peak at 412 nm developed, which was ascribed to an increase in the 'molecular rigidification' or 'conformational restriction' of the theophyllinium moiety.

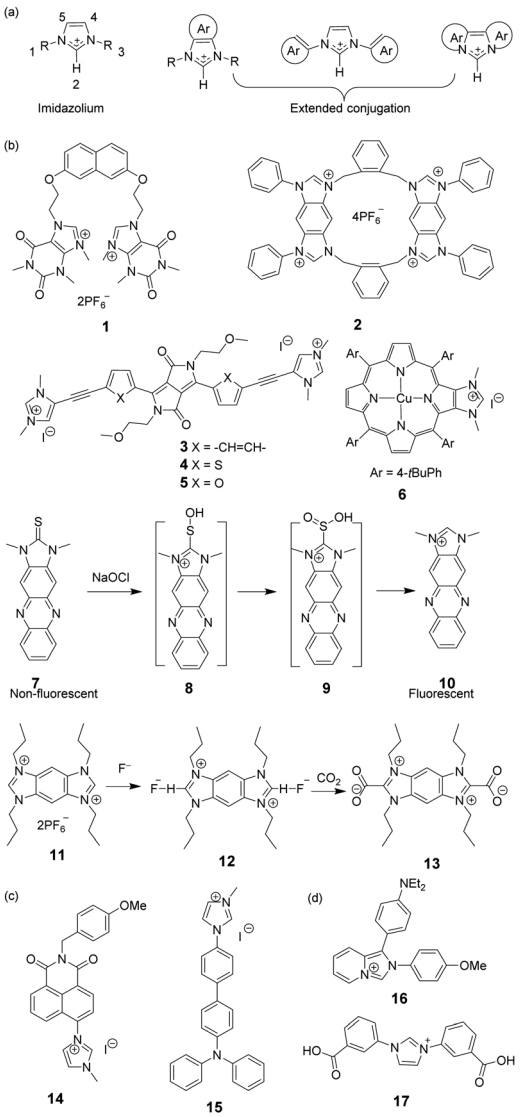

Fig. 1 (a) The general structures of extended imidazolium conjugated systems; and (b and c) structures of compounds **1–17**.

Yoon and co-workers reported a cyclic benzobisimidazolium receptor **2** (Fig. 1b), which effectively recognized HSO_4^- in aqueous solutions *via* changes in fluorescence and UV absorption.[11] The two imidazolium moieties in receptor **2** played an important role in generating neutral CH···O hydrogen bonds and stabilizing the complex. Specifically, the proximate imidazolium moieties enhanced C–H hydrogen bonding. The pre-organized and rigid binding pocket in **2** provided four aryl C–H and four benzylic C–H hydrogen bonds with HSO_4^-.

Gryko and co-workers connected 1,3-dimethylimidazolium cationic units with diketopyrrolopyrrole *via* benzene (**3**), thiophene (**4**), and furan rings (**5**) as π spacers (Fig. 1b).[12] The new fluorophores exhibited large two-photon absorption cross-sections (4000 GM) and very high two-photon brightness values exceeding 2000 GM. The charged nature of the imidazolium moiety in these substances makes them useful in mitochondrial staining of living cells.

A system comprised of porphyrin **6** (Fig. 1b) fused across the β,β-pyrrolic positions of an imidazolium ring has been described by Richeter and co-workers.[13] Even though only the electrochemical properties of **6** were investigated using cyclic and rotating disk voltammetry, the optical features of the porphyrin moiety make this compound a candidate for use as an anion sensor.

Yoon and co-workers designed imidazoline-2-thione **7** (Fig. 1b) as a fluorescent probe for OCl^-.[14] The probe displayed a highly selective and sensitive fluorescence turn-on response to OCl^-, and it can be utilized to image OCl^- generation in macrophages co-cultured with HeLa cells. More importantly, **7** can be utilized in combination with two-photon microscopy (TPM) to image OCl^- in cells and tissues. The TP action cross-section value of **7** in EtOH was determined to be 0.4 GM at 800 nm, whereas the δ_{max} value was 42 GM.

Yoon and co-workers reported that the tetrapropyl benzo bisimidazolium system **11** (Fig. 1b) serves as a fluorescent and colorimetric sensor for CO_2.[15] The system utilized fluoride to activate a tetrapropyl-benzobisimidazolium salt and operates in the absence of an exogenous base. The mode of action of **11** is ascribed to the fluoride-induced formation of an N-heterocyclic carbene intermediate that reacts with CO_2 to form an imidazolium carboxylate **13**. The system featured high selectivity for fluoride, a low limit of detection (30 ppm), a fast response time and an ability to have both fluorescence and colorimetric outputs.

The most convenient way to extend imidazolium aromatic systems is to link a chromophore to the nitrogen of the imidazole ring (Fig. 1c). Using this approach, Frontera and co-workers connected an imidazolium group to the 4-position of 1,8-naphthalimide to produce **14**.[16] Binding with anions influences the internal charge transfer characteristics of **14**, which gives rise to optical signals. Probe **14** is a highly selective

colorimetric and ratiometric 'off–on' signaling sensor targeting F^-. Importantly, Cl^-, Br^-, I^-, HSO_4^-, SCN^-, AcO^-, and NO_3^- do not appreciably alter the photophysical properties of the probe even at relatively high concentrations (10 equiv.). The detection limit for F^- was 3.86×10^{-6} M. A large downfield shift of the imidazolium C(2)–H resonance in the ^{1}H-NMR spectrum confirmed the strong binding affinity of **14** with F^-.

You and co-workers developed **15** (Fig. 1c) in which the biphenyl group bridged the diphenylamino group and the imidazolium group.[17] This substance exhibited high selectivity and a fluorescence turn-on response for $H_2PO_4^-$ in acetonitrile and for ClO_4^- in water. The fluorescence changes were due to the twisted intramolecular charge transfer (TICT)-controlled aggregation-induced emission (AIE) effect.

Imidazo[1,5-*a*]pyridinium ion **16** (Fig. 1d) was reported to be an interesting fluorophore by Aron and co-workers.[18] This compound has a relatively low pK_a value and operates as a pH-sensitive probe in either a ratiometric fashion for precise determination of local pH values or in a turn-on/off fashion for visualization/imaging with high spatial resolution.

Liu and co-workers assembled a 2D lanthanide coordination polymer {Eu-CP**17**} (Fig. 1d) based on the solvothermal reaction of an imidazolium-based dicarboxylic acid ligand **17**.[19] In their work, **17** revealed the representative red luminescence of Eu^{3+} ions upon excitation at 308 nm. The luminescence tests indicated that **17** has excellent selectivity and sensitivity to detect Fe^{3+}/Fe^{2+}, $Cr_2O_7^{2-}$, and a series of nitroaromatic explosives (NAEs), quenching the luminescence emission of **17** at 618 nm. The limits of detection of **17** to detect Fe^{3+}/Fe^{2+} and $Cr_2O_7^{2-}$ could reach 5×10^{-7} M and 1×10^{-6} M, respectively. The quenching efficiency for the various NAEs can reach 90%. More importantly, **17** could be regenerated and reused at least five times by simple post-processing.

2.2 Alkylimidazolium

Imidazolium ions have both charge and C_2–H hydrogen-bond-donor properties that enable them to bind anions. In contrast to that of conventional hydrogen bonds, the orientation dependence of the H-bond interactions between C_2–H and an anion is low. It is believed that C_2–H was not the key factor influencing the binding ability. In contrast, recent studies have demonstrated that substitution of C_2–H by other functional groups, such as alkyl and halo-groups (the next sub-section), strengthens the binding affinities with anions. Beer *et al.* explored the participation of 2-methylimidazolium in anion templated pseudorotaxanes and rotaxanes.[20] In spite of gaining evidence supporting this conclusion for solid-state systems, no interactions were found to exist between the methyl protons of the imidazolium ring and anions in the solution phase. In a recent study,[21] a two-armed 2,4,5-trimethylimidazolium-based oxoanion receptor **18** (Fig. 2), which incorporates two end capped photoactive anthracene rings, was prepared. ^{1}H- and ^{31}P-NMR studies with this substance clearly indicate the simultaneous occurrence of several charge-assisted aliphatic and aromatic C–H non-covalent interactions with the imidazolium C(2)–CH_3 protons, the methylene N–CH_2 protons and the inner aromatic proton or the outer heteroaromatic

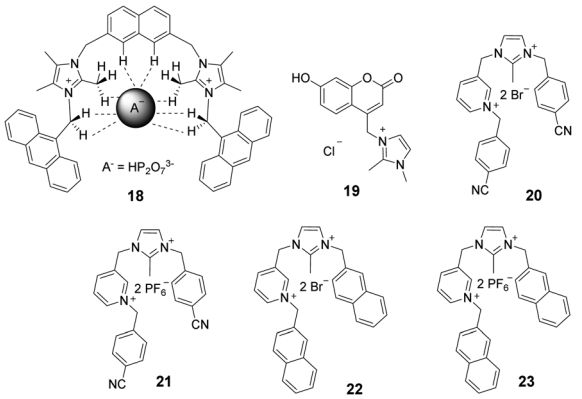

Fig. 2 Structures of compounds **18–23**.

protons. In addition, a fluorescent coumaryl linked 2-methylimidazolium salt **19** (Fig. 2) provided highly selective nanomolar detection of a commonly used explosive (picric acid) over other aromatic explosives in aqueous media.[22] The results of UV-vis, time resolved fluorescence and DFT studies show that ground-state electron transfer from the picrate anion to this sensor is the predominant mechanism for fluorescence quenching.

Milton and co-workers synthesized two aryl-functionalized water-soluble unsymmetrical *N*,*N*′-disubstituted imidazolium bromide salts (**20** and **22**) and studied their counter anion exchange to hexafluorophosphate salts (**21** and **23**) (Fig. 2).[23] Therein, **20** and **21** displayed emission maxima at 297 nm and probes **22** and **23** displayed emission maxima at 335 nm. These probes selectively detected Fe(III) ions over other metal ions in the physiological pH range by a fluorescence "turn-off" mechanism. The Job plot studies of **20**–Fe^{3+} indicated a stoichiometry of 1 : 1. The detection limit and binding constant for the **20**–Fe^{3+} complex were calculated to be 2.81×10^{-5} M and 1.51×10^4 M, respectively.

2.3 Halo-imidazolium

Bonding between an electron-deficient halogen atom and a Lewis base has attracted much interest as an effective interaction to exploit for anion recognition.[24] Beer and co-workers synthesized a bidentate bromoimidazoliophane **24** (Fig. 3) and found that it displayed selective binding with Br^- *via* halogen bonding in aqueous solution.[25] The two bromoimidazolium groups in compound **24** interact with one bromide ion. Because the bromoimidazolium rings point towards a bromide ion, the structure of **24** has a calix-like shape leading to an open cleft on the other side of the macrocycle. After the addition of bromide, the halogen-bonded bromide ion of an adjacent molecule could occupy this space, leading the calixes to stack into one another. Based on the results of ^{1}H NMR titrations in CD_3OD/D_2O (9 : 1, v/v), chloride ions caused a moderate downfield shift of the signals, iodide ions caused a slight downfield shift, and fluoride ions showed no changes. The association constant of **24** for the halide was calculated to follow a binding trend of Br^- (889 M^{-1}) > I^- (184 M^{-1}) > Cl^- (<10 M^{-1}) > F^-. Non-covalent bonding interactions between the Br on the receptor

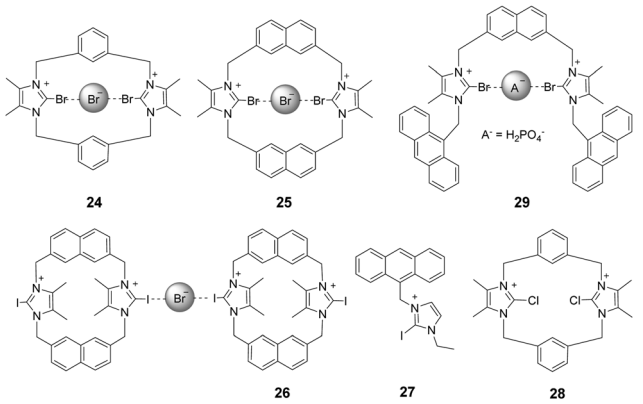

Fig. 3 Structures of compounds **24–29**.

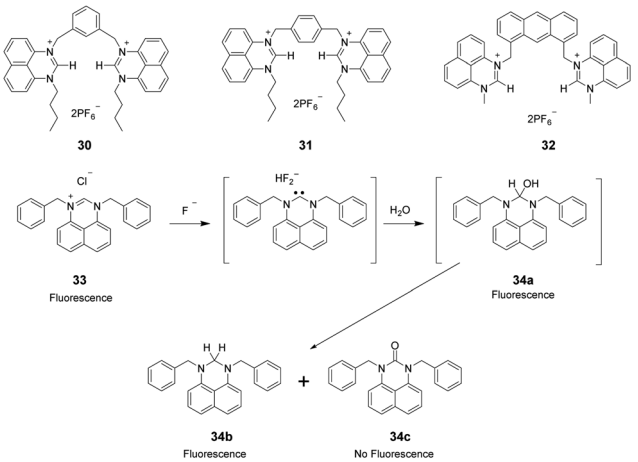

Fig. 4 Structures of compounds **30–34**.

and Br^-, so-called halogen bonding, are thought to play a key role in this interaction. Br atoms on the imidazolium act as halogen bonding donors and at the same time cause significant steric influence.

By replacing the benzene ring with a naphthalene ring, Beer and co-workers prepared a series of novel macrocyclichaloimidazolium receptors, which contain chloro-, bromo- (**25**), and iodo-imidazolium (**26**) motifs (Fig. 3).[26] The results of ^{1}H NMR titration experiments on aqueous solutions (CD_3OD/D_2O = 9 : 1) showed that the protons of naphthalene in receptors **25** exhibited significant downfield shifts upon addition of Br^- anions. This change was accompanied by an *anti*/*syn* conformer ratio change from 25 : 75 to 8 : 92. Addition of I^- anions caused similar changes. Receptor **26** exhibits the same trend as **25**; the addition of Br^- to a solution of **26** induced a red-shift of the emission peak at 401 nm with a new peak appearing at 437 nm. The association constants for **26** with Br^- and I^- were calculated to be 9.55×10^5 M^{-1} and 3.71×10^4 M^{-1}, respectively.

Studies of the anion binding properties of 2-iodo-imidazolium receptors **26**[26] and **27**[27] and 2-chloro-imidazolium receptors **28**[26] (Fig. 3) have provided results that enable full attribution of the observed affinities to strong charge-assisted C–I$\cdots$$X^-$ and C–Cl$\cdots$$X^-$ halogen bonding, respectively.

Molina and co-workers reported a two-armed 2-bromo-imidazolium-based anion receptor **29** (Fig. 3), which acted as a selective fluorescent sensor for $H_2PO_4^-$ anions. In this case, only $H_2PO_4^-$ promoted the appearance of the anthracene excimer emission band, whereas the emission from **29** remained unchanged in the presence of other tested anions.[28] Compared with those of the hydrogen-bonding counterparts, the association constants of the halogen-bonding complexes in CD_3CN/MeOD (8/2) with $H_2PO_4^-$ and SO_4^{2-} anions are much larger.

2.4 Perimidinium

Perimidinium ions have a structure similar to imidazolium ions. As a result, perimidinium is also anticipated to form (C–H)$^+\cdots$$X^-$ type ionic hydrogen bonds with anions. Also, its large aromatic system makes perimidinium an excellent intrinsic chromophore. Gao and co-workers reported two perimidinium-based receptors **30** and **31** (Fig. 4), which exhibit good selectivity for acetate by evaluation with UV-vis, fluorescence, and ^{1}H NMR.[29] This effort demonstrated that (C–H)$^+\cdots$$X^-$ type ionic hydrogen bonding between the perimidinium moieties and acetate plays a crucial role in anion recognition. In a later study, the same group reported that another perimidinium cation **32** (Fig. 4) is an efficient fluorescent and colorimetric chemosensor for F^- in DMSO containing 10% water.[30] Upon addition of F^-, the yellow and non-fluorescent solution of **33** became colorless and exhibited strong blue fluorescence. The change is due to the formation of an N-heterocyclic carbene by F^--promoted deprotonation, which immediately reacted with water to give a colorless and fluorescent carbinol **34a**, which is further disproportionated to generate the fluorescent **34b** and the non-fluorescent **34c** (Fig. 4).

Kang and co-workers synthesized the two-perimidinium-armed anthracene derivative **32** (Fig. 4). This receptor was found to bind basic anions weakly through both aromatic C–H (two perimidine C_2–H, anthracene 9-H) and aliphatic C–H (two perimidine 1-methyl C–H, two benzylic C–H) hydrogen bonding interactions.[31]

3. Receptor scaffolds

3.1 Diimidazolium receptors

Kumar and co-workers reported a 1-(4-biphenyl)benzimidazolium based dipodal system **35** as a fluorescent chemosensor for the detection of perchlorate.[32] The benzimidazolium groups of **35** (Fig. 5) provide multiple C–H/O recognition sites for ClO_4^- anions. The formation of a 1 : 1 stoichiometric complex of **35**–ClO_4^- was confirmed using a Job plot, ^{1}H NMR titration studies and X-ray crystal structure analysis. The detection limit of **30** for ClO_4^- was determined using a fluorescence titration method to be 100 nM, which is much lower than the permissible perchlorate concentration of 150 nM in drinking water.

Yoon and co-workers developed the boronic acid-based fluorescent probe **36** (Fig. 5) bearing two imidazolium groups and two pyrene groups. Among various dopamine derivatives,

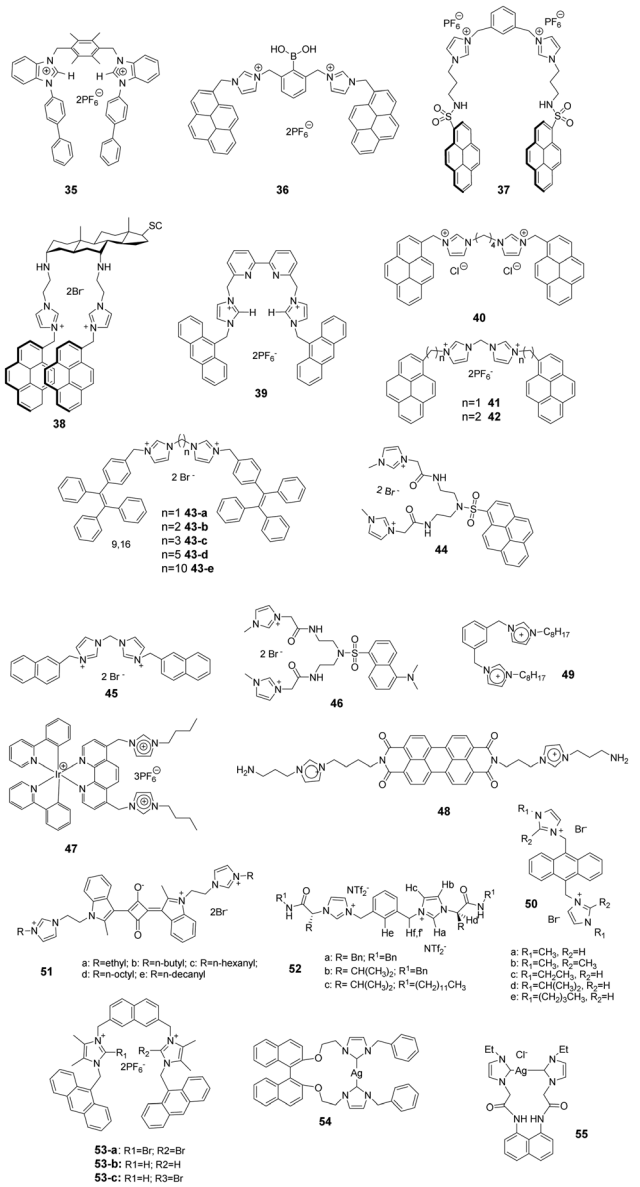

Fig. 5 Structures of compounds **35–55**.

3,4-dihydroxyphenylacetic acid (DOPAC) exhibited the strongest binding to **36** in HEPES (0.02 M, pH 7.4)–CH_3CN (95 : 5, v/v).[33] The association constant for DOPAC was calculated to be 1.72×10^4 M^{-1}, and those for catechol, dopamine, and L-DOPA were 4.38×10^3 M^{-1}, 4.13×10^2 M^{-1} and 2.08×10^3 M^{-1}, respectively. The specific intermolecular excimer formation and fluorescence quenching effects induced by binding with DOPAC and catechol were explained using theoretical calculations.

Kim and co-workers reported that the *N*-imidazolylpropylpyrene sulfonamide based diimidazolium salt **37** (Fig. 5) can be used for sensing cyanide anions in PBS–EtOH solution (pH = 7.4).[34,35] A dramatic quenching of both the monomer (379 nm) and excimer emission (495 nm) of probe **37** occurred in the presence of CN^- due to the unlocking of the π–π interactions. The formation of a 1 : 2 complex between **37** and CN^- was confirmed using a Job plot, and the association constant was determined to be 2.32×10^5 M^{-1}. Kim and co-workers also utilized this diimidazolium salt for selective detection of 3,5-dinitrosalicylic acid (3,5-DNSA) in a PBS–EtOH (v/v = 1 : 9, pH 7.4) solution. The interaction between 3,5-DNSA and **37** was examined using UV-visible, fluorescence and ^{1}H NMR spectroscopy. This substance showed a large association constant with 3,5-DNSA ($K_a = 8.16 \times 10^4$ M^{-1}) with a 1 : 2 stoichiometry.

Kim's group also synthesized the cholestane derivative **38** bearing an imidazolium pyrene moiety as a fluorescent receptor for dicarboxylates.[36] Upon excitation at 344 nm, **38** (Fig. 5) displayed monomer emission between 380 and 420 nm and excimer emission at 481 nm. Receptor **38** displayed decreasing binding affinities with various carboxylate anions in the order oxalic acid > D-tartaric acid > L-tartaric acid > maleic acid > fumaric acid > malonic acid > succinic acid > glutaric acid. The binding constant between **38** and oxalic acid was calculated to be 5.06×10^4 M^{-1}.

To take advantage of subtle variations in the binding site of the anthracene-coupled benzimidazolium fragment, Yoon and co-workers applied this fragment to design the new anthracene-based fluorescent probe **39** (Fig. 5).[37] This chemosensor showed photo-induced electron transfer (PET) behavior promoted by anion recognition. For example, the addition of PPi or $H_2PO_4^-$ induces a highly selective fluorescence quenching effect with the formation of a unique excimer peak around 480 nm. The association constants of **39** with PPi and $H_2PO_4^-$ were 6.19×10^6 M^{-1} and 4.68×10^5 M^{-1}, respectively.

Fang and co-workers developed fluorescent sensor **40** (Fig. 5) for the detection of explosives in aqueous solutions. This sensor consisted of an assembly of different surfactants (sodium dodecyl sulfate (SDS), dodecyl trimethylammonium bromide (DTAB) and Triton X-100 (TX100)) as micellar solutions.[38] Picric acid (PA) induced the largest fluorescence quenching of **40** in the anionic **40**/SDS system, which was due to electrostatic attraction of the phenoxide with the fluorophore located on the micelle surface. In contrast, other analytes were encapsulated in the SDS micelles. In cationic DTAB micelles, **40** displayed the highest on–off fluorescence responses to PYX. This phenomenon could be due to the fact that the fluorophore is not well incorporated in the DTAB micelles, while PYX can freely access the fluorophore.

As antibiotic resistance increases, bacterial infections are major factors threating human health. Therefore, it is meaningful to develop a method for rapid and efficient identification and imaging of bacteria. Imidazolium is a good receptor that recognizes bacteria. Xu's group developed imidazolium-derived pyrene sensors **41** and **42** to rapidly identify and quantify different bacteria species *via* the synergistic effects of electrostatic interactions and hydrophobic forces.[39–41] The compounds aggregated to form nanoparticles and the fluorescence was quenched by aggregation effects. After the addition of bacteria, nanoaggregates bound the anionic bacteria surface and disassembled to form various combinations of pyrene monomer and excimer binding modes. The output signals of the emission profiles showed two channels of fluorescence

increase and ratiometric change, which could be used to generate a two-dimensional analysis map for bacteria identification. Sensor **42**, which had longer spacers between imidazolium and pyrene, was more sensitive than **41**. Fourteen clinically isolated multidrug-resistant bacteria and their staining properties were rapidly identified by **42**.

Cao and co-workers designed and synthesized a series of AIE-based tetraphenylethene (TPE) appended linear bis-imidazolium salts with different chain length spacers.[42,43] All the bis-imidazolium salts showed good solubility in aqueous solutions with weak fluorescence and showed selective fluorescence enhancement based aggregation-induced emission at 471 nm toward ATP, ADP and PPi, particularly ATP anions. It was found that the two imidazolium units played a key role for binding the triphosphate anion of ATP *via* ^{1}H NMR titration and DLS experiments. The binding affinity of the probes toward ATP decreased with increasing linker chain length, with the binding constants following the order of **43-a** (1.19×10^5 M^{-1}) > **43-b** (1.06×10^5 M^{-1}) > **43-c** (1.93×10^4 M^{-1}) > **43-d** (1.75×10^4 M^{-1}) > **43-e** (1.46×10^4 M^{-1}). In addition, **43-a** and **43-b** (with the shorter chain length spacers) showed a moderate fluorescent turn-on response toward PPi, and **43-c** was successfully used for fluorescence imaging of intracellular ATP in live cells.

Fang and co-workers developed an imidazolium-modified pyrene derivative as a ratiometric fluorescent sensor **44** for detection of heparinin in both aqueous solutions and serum samples.[44] The probe showed blue-to-green emission change interactions with heparin *via* electrostatic interactions, and the binding constant was calculated to be 3.9×10^6 M^{-1}. Furthermore, **44**/heparin could detect protamine, leading to a green-to-blue emission change, since protamine replaces **44** to bind heparin due to the stronger affinity of heparin with protamine. The detection limits of heparin and protamine were measured to be 8.5 (153 ng mL^{-1}) and 15.4 nM (107.8 ng mL^{-1}), respectively.

Graphene complexes with imidazolium-based salts showed strong visible fluorescence and special functions. Ahmed's group designed an acyclic water-soluble naphthaimidazolium chemosensor **45** to show selective turn-on fluorescence for RNA at physiological pH in aqueous solution.[45] Moreover, the compound could be utilized to produce a fluorescent graphene complex with high quantum yield (0.87) *via* a simple ion-exchange strategy. Because the chemisorbed imidazolium hinders the electron transfer between the naphthalene moiety and graphene, the fluorescent graphene complex displayed a close resemblance to the water-soluble fluorescent chemosensor in its electronic state.

Ding and co-workers synthesized a supramolecular binary ensemble based on cationic dansyl derivative **46** with imidazolium-modified and anionic surfactant (SDS) assemblies, which displayed selective turn-off responses to aspartic acid (Asp) and glutamic acid (Glu) in aqueous medium.[46] Time-resolved decay measurements showed that the quenching by Asp and Glu was static in nature, and the specific binding of H^+ released from Asp and Glu with the dansyl alkylamine was responsible for the fluorescence quenching *via* fluorescence titration, absorption titration and ^{1}H NMR studies. The detection limits for Asp and Glu were 0.6 μM and 2.1 μM, respectively.

Schmittel and co-workers developed the iridium(III)-imidazolium based lab-on-a-molecule multianalyte sensor **47** (Fig. 5), which can detect three different anions using three channels.[47] The iridium complex **47** displays a new CT band in the UV-vis channel at 457 nm upon addition of F^- ($\log\beta$ = 9.71 ± 0.30), which was suggested to be a consequence of the formation of a new electron-donating unit. As detected in the photoluminescence channel, $H_2PO_4^-$ ($\log\beta$ = 7.18 ± 0.10) induces a selective increase in emission along with a blue-shift from 660 nm to 607 nm due to an increase in the energy gap between the auxiliary ligand (^{3}LX) and the ground state. Finally, complex **47** undergoes a high electrochemiluminescence enhancement at 602 nm in the presence of AcO^- with a detection limit of 0.17 mM.

Niu and co-workers designed and prepared a new perylene-diimide (PDI) derivative **48** (Fig. 5) by grafting the PDI core with two ionized amino-imidazole arms.[48] The presence of the π-conjugated PDI core endowed it with the ability to self-assemble. Furthermore, **48** undergoes a reversible conversion of its fluorescence emission and super-molecular structure in response to pH changes. By increasing the pH from 4.0 to 7.0, the emission peaks at 549 nm and 590 nm decreased gradually, which suggests that **48** changes from a monomer-state (FL-On) to an aggregated-state (FL-Off). It was also found that its behavior as a fluorescent on–off sensor upon pH stimulation was reversible. Transmission electron microscopy analysis of this substance at different pHs showed that **48** existed as short nanobelts (50 nm) at pH 4.0 due to protonation of the amine group, which generated large intramolecular repulsive interactions. In contrast, its structure changed to long and highly branched nanobelts due to deprotonation of the ammonium ion when the pH increased to 7.0.

Noto and co-workers examined the anion recognition ability of the diimidazolium pincer **49** (Fig. 5) in acetonitrile using NMR analysis.[49] Simple inorganic ions, such as halide, and mono- and dicarboxylate anions, were examined. The order of binding of **49** with halide ions was $Cl^- > Br^- > I^-$. Moreover, **49** displayed higher binding abilities to dicarboxylate anions with the trend of tartrate ($K > 10^4$) > succinate (K = 8000) > oxalate (K = 1000) > fumarate (K = 150), whereas monocarboxylates induced a negligible response. The selectivity was caused by the stability of the complex, which was determined by the relationship between the size and the flexibility of dicarboxylate anions.

Li and co-workers synthesized a novel series of anthracene imidazole ionic liquids **50** (Fig. 5) as efficient fluorescent probes for detecting superoxide anion radicals ($^\bullet O_2^-$) in aqueous systems.[50] The species $^\bullet O_2^-$ can easily destroy the π-bond structure in **50** by oxidizing the imidazole cation, which leads to a large fluorescent decrease at 422 nm. The relationship between the relative fluorescence intensity (ΔF) and the concentration of $^\bullet O_2^-$ showed good linearity in the range of 1–70 μM in Tris–HCl buffer (0.10 M, pH 8.2) at room temperature. The detection limit of the probe for $^\bullet O^{2-}$ was 0.7 μM.

Chen and co-workers synthesized a series of water-soluble imidazolium-anchored squaraine dyes **51** (Fig. 5) and subjected them to UV-vis and fluorescent spectroscopy studies in aqueous media (D-HBSS).[51] It was found that an increase in the length of the alkyl chain in these substances leads to a decrease in the aggregate band at 540 nm and an increase in the monomer band at 574 nm. Accordingly, the fluorescence intensity exhibited a gradual enhancement upon lengthening the alkyl chain. The dyes were also utilized for bioimaging. The results demonstrated that **51d** serves as a fluorescent probe for live cell imaging with good cellular uptake and staining. More interestingly, the fluorescence of **51d** was quenched by both Fe^{2+} and H_2O_2, which was attributed to the formation of the hydroxyl radical in the Fenton reaction.

Transport of chloride across cell membranes is an essential event in numerous biological processes. Luis and co-workers reported a new class of bis(imidazolium) salt-based anion transporters **52** (Fig. 5).[52] As an extension of their previous work,[53] ^{1}H NMR spectroscopy, ESI-MS and computational techniques were used to investigate the inorganic anion complexing properties of these transporters. Transporter **52** displayed a strong interaction with chloride anions, reflected in the formation of a stable 1 : 1 complex with an association constant K_a of 1585 M^{-1}. The results of trans-membrane chloride transport studies revealed that **52a** has a higher exchange mechanism chloride transport activity than that of **52b** and **52c**, which demonstrated that the participation of hydrogen bond interactions of aromatic spacers might provide the most stable disposition for coordinating anions.

The hydrogen bond (HB) and halogen bond (XB) of imidazolium have been the most non-covalent interaction applied in the design of anion receptors. Molina and co-workers synthesized a series of two-armed imidazolium-based naphthalenes with two photo active anthracenes to study the halogen bonding interactions in combination with others in the anion recognition process.[54,55] The structures of the charge-assisted bidentate receptors involved 2-bromo-bonding (**53-a**), hydrogen-bonding (**53-b**) or both halogen and hydrogen bonding (**53-c**) site imidazolium receptors. Spectroscopic measurements and ^{1}H and ^{31}P-NMR studies showed that only $HP_2O_7^{3-}$, $H_2PO_4^-$, SO_4^{2-} and F^- anions promoted noticeable changes among a wide variety of anions investigated. Higher association constants for the receptors **53-a** and **53-b** were found for the $H_2PO_4^-$ anion, but for receptor **53-c**, it was more selective for the SO_4^{2-} anion.

Wang and co-workers obtained compound **50** *via* the reaction of bis-imidazolium salts (*S*)-2,2′-bis[2″-(*N*-R-imidazoliumyl)-ethoxy]-1,1′-binaphthyl hexafluorophosphate [R = benzyl] with Ag_2O in $ClCH_2CH_2Cl$/DMSO.[56] Interestingly, the macrometallocycle **54** can selectively and sensitively detect $H_2PO_4^-$ from other anions based on a remarkable decrease in the fluorescence intensity of **54** during fluorescence and UV/vis spectroscopic titration measurements. This phenomenon might be attributed to the switch-on of the PET process from the imidazole ring to the binaphthyl in the presence of $H_2PO_4^-$. The detection limit was estimated to be 4.9×10^{-8} mol L^{-1}.

Liu and co-workers synthesized an N-heterocyclic carbene (NHC) metal complex **55** with a groove-like 14-membered macrometallocycle,[57] and the macrometallocycle consisted of one biscarbene ligand and one silver(I) ion. The fluorescence, ultraviolet spectroscopy, ^{1}H NMR titrations, MS and IR spectra showed that **55** can selectively and sensitively detect Cu^{2+} from other cations, and **55** bound with Cu^{2+} mainly through $Cu^{2+}\cdots O$ and $Cu^{2+}\cdots N$ interactions. The K_{SV} value of **55** for Cu^{2+} based on a 1 : 1 association equation analysis was determined to be 5.68×10^5 M^{-1}, and the detection limit was 1.5×10^{-7} mol L^{-1}.

Kumar and co-workers introduced bis-benzimidazolium groups into the 9- and 10-positions of anthracene to create probe **56** (Fig. 6).[58] Among various anions, acetate in 90% aqueous buffer (pH 7.4, 10% DMSO) caused a large fluorescence quenching effect on this probe. Titration of **56** with KOAc showed that a 1 : 1 stoichiometric complex is formed with a binding constant $\log \beta_{L(AcO)} = 5.20 \pm 0.03$.

Yoon and co-workers also combined phenylboronic acid with two naphthoimidazolium groups to construct the ratiometric fluorescent probe **57** (Fig. 6) for fluoride ions.[59] Gradual

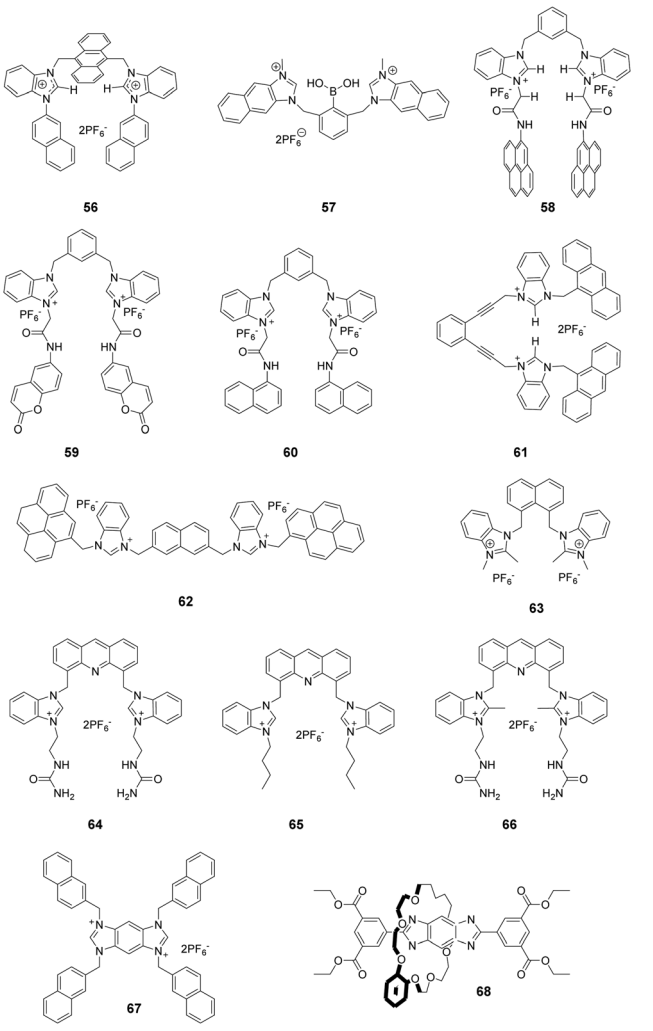

Fig. 6 Structures of compounds **56–68**.

addition of F^- to **57** induced a significant decrease in the 445 nm emission and a blue-shift as well as an increase in the emission band at 370 nm. These were attributed to the formation of a **57**/F^- complex. The emission shift was caused by hydrogen bonding between C_2–H and fluoride. The association constant of the complex between **57** and F^- was calculated to be 2.3 ($\pm$0.2) $\times$ 10^6 M^{-1}.

Ghosh and co-workers reported that the benzimidazolium-based chemosensor **58** (Fig. 6), which contained appended pyrene groups, can distinguish between $H_2PO_4^-$ and F^- in CH_3CN.[60] Among various anions, $H_2PO_4^-$ induced a decrease in the intensity of the monomer (384 and 403 nm) emission band of **58** and an increase of its excimer emission band (482 nm). This specific response is due to the strong hydrogen bonding interaction occurring between $H_2PO_4^-$ and **58**. On the other hand, F^- ions result in efficient fluorescence quenching of both the monomer and excimer emission of the probe because of deprotonation of the amide protons. The association constants for the formation of the complex of **58** with $H_2PO_4^-$ and F^- were determined to be 2.23 $\times$ 10^4 M^{-1} and 8.88 $\times$ 10^3 M^{-1}, respectively. Moreover, quenching of the fluorescence of **58** can also be used to distinguish AMP from ATP and ADP in CH_3CN–H_2O (1 : 1, v/v) at physiological pH 7.3.

In an extension of this work, Ghosh and co-workers replaced the appended pyrene groups in **58** with coumarin motifs and naphthalene motifs to create the new receptors **59** and **60**, respectively (Fig. 6), which displayed fluorometric recognition of anions in CH_3CN under different conditions.[61] Receptor **59** exhibited a selective fluorescence enhancement upon addition of lower equivalent amounts of hydrogen pyrophosphate ($HP_2O_7^{3-}$) (K_a = 4.10 $\times$ 10^4 M^{-1}), while receptor **60** showed selective enhancement of the emission at 510 nm in the presence of F^- (K_a = 4.11 $\times$ 10^3 M^{-1}). The difference in selectivity of receptors **59** and **60** was due to the different dispositions of the appended fluorophores, which regulated the dimensions of the pseudo cavities where anion binding takes place. On the other hand, **59** displayed a preference for ATP with a binding constant of 2.85 $\times$ 10^3 M^{-1} in aqueous CH_3CN.

Ghosh and co-workers developed another $H_2PO_4^-$ chemosensor **61** (Fig. 6) in which two benzimidazolium motifs are linked to an enediyne scaffold.[62] In the presence of $H_2PO_4^-$ ions, the monomer emission of **61** decreased and a new peak appeared at 500 nm. This characteristic emission change was attributed to chelation induced excimer formation between the closely spaced anthracene moieties. The 1 : 1 stoichiometry of the complex of **61** with $H_2PO_4^-$ was determined using a Job plot, and the binding constant was determined to be 3.06 $\pm$ 0.6 $\times$ 10^4 M^{-1}.

Molina and co-workers described the bis-(benzimidazolium) receptor **62** (Fig. 6).[63] The results of fluorescence and NMR spectroscopy studies showed that **62** exhibits good recognition properties towards sulphate and hydrogen pyrophosphate anions in aqueous media (DMSO : H_2O = 9 : 1). Job plot analysis of **62** with SO_4^{2-} and $HP_2O_7^{3-}$ revealed the formation of a 1 : 1 receptor to anion-binding stoichiometry. The association constants of **62** were calculated to be 2100 M^{-1} and 357 M^{-1} for SO_4^{2-} and $HP_2O_7^{3-}$, respectively. A large downfield shift of the C_2–H protons in the ^{1}H NMR spectrum of **62** confirmed that a strong binding interaction occurs with SO_4^{2-} and $HP_2O_7^{3-}$, which induces a remarkable increase in the intensity of both the monomer (379, 397 and 418 nm) and excimer (481 nm) bands.

The novel anion receptor **63** (Fig. 6), which is based on 2-methyl benzimidazole, was synthesized by Kang and co-workers.[64] UV-vis, fluorescence and ^{1}H NMR spectroscopy were used to investigate the binding characteristics of this substance. The emission intensity of **63** at 347 nm gradually decreased upon addition of increasing concentrations of tetrabutylammonium acetate, which indicated the presence of a hydrogen bond interaction between the C–H hydrogen and acetate ions. The association constant was calculated to be 1.0 $\times$ 10^4 M^{-1} using fluorescence titration. In addition, the binding affinity order for halides is $Br^- > Cl^- > I^-$ (as determined by ^{1}H NMR titration), which reflects the sizes and basicities of the halides.

Gao and co-workers reported three tweezer-like fluorescent sensors **64–66** (Fig. 6), all of which contain an acridine fluorophore. The side chain pendants in **64** and **66** contain urea moieties, whereas **65** (containing alkyl side chains) was used as a control to investigate possible synergistic effects.[65] The anion binding affinities of these probes were evaluated using fluorescence spectroscopy. By addition of $H_2PO_4^-$, receptor **64** displayed a significant fluorescence decrease at 430 nm and an increase at 480 nm. The new emission peak at 480 nm was due to excimer formation between two acridine fluorophores induced by binding of $H_2PO_4^-$. Receptor **64** also exhibited fluorescence quenching upon addition of HSO_4^- due to a PET process. The binding constants between sensor **64** and $H_2PO_4^-$ and HSO_4^- were 5.1 $\times$ 10^4 M^{-1} and 1.7 $\times$ 10^6 M^{-1}, respectively.

Yoon and co-workers reported a benzobisimidazolium derivative (**67**) bearing four naphthalene moieties as an F^- ion-selective fluorescent chemosensor.[66] Compound **67** exhibited strong fluorescence at 430 nm in the presence of F^- and $CH_3CO_2^-$ resulting from stable aggregates formed due to electrostatic interactions between the positively charged benzobisimidazolium moieties and anions in CH_3CN. Furthermore, the fluorescence of the aggregates was further enhanced in CH_3CN with the presence of 5% water, which can be attributed to aggregation-induced emission.

Mapping the free-energy landscape provides an understanding of the energetic barriers to shuttling and helps identify the stable and metastable structures. Cai and co-workers investigated a rotaxane-based molecular shuttle **68** to decipher the molecular mechanism of the pH-controlled optical switch.[67] The rotaxane structures were composed of a benzo[24]crown-6 ether wheel threaded onto an axle with a benzo-bis(imidazolium) core. The pH-dependent three-dimensional free-energy calculations showed that isomerization of the macrocycle played a central role in regulating the fluorescence of the rotaxane. π-Stacking of the wheel aromatic rings and the benzo-bis(imidazole) core of the axle led to fluorescence quenching of the protonated rotaxanes at low

pH. Furthermore, the substituent group on the aromatic ring of the crown ether also influenced the π-stacking structure, which can provide a theoretical basis for the design of tailored optical switches.

Liu and co-workers synthesized a series of alkylmethyl imidazolium derivatives bearing ferrocene moieties (**69–72**) (Fig. 7) that can electrochemically recognize various anions as a consequence of electrostatic attraction.[68] Analysis using cyclic voltammetry (CV) and Osteryoung square-wave voltammetry (SWV) showed that all the receptors except **66a** exhibited selective binding with anions in the order $F^- > Cl^- > Br^-$, which followed the halide negative charge density order. Among the receptors, **69a** and **70a** showed much stronger sensing properties for F^- in CH_3CN, which was due to the presence of a ferrocene center directly linked to the methylimidazolium moieties. In contrast, the bis-substituted receptors undergo a larger potential shift than the monosubstituted receptor in the presence of F^- (*e.g.* $\Delta E_{1/2}$(**69a**) = 230, $\Delta E_{1/2}$(**70a**) = 270 mV).

Yuan and co-workers reported a study using acyclic ferrocene derivatives **73–76** (Fig. 7) containing ferrocenyl-methyl imidazolium groups connected through flexible or rigid spacers.[69] The electrochemical properties of these receptors were investigated using cyclic voltammetry. These substances displayed typical "two wave behavior". Upon addition of anions, the peak of the free receptor gradually decreased, and a new wave appeared at more negative potential. This change was attributed to a hydrogenation reaction occurring at the iron center. More interestingly, the flexible receptor containing probes **73** and **74** undergo larger potential shifts than do the rigid receptors **75** and **76** because their flexibility enables their structures to change during the processes of recognizing anions. New peaks appeared at $\Delta E_{1/2}$ = −212, −201, −164 and −168 mV, respectively, for receptors **73–76** upon addition of F^-. The results of ^{1}H NMR titrations showed that the order of anion binding to receptors **73–76** in DMSO-d_6 is $AcO^- > Cl^- > Br^- > HSO_4^- > I^-$.

As an extension of their work, Yuan and co-workers also synthesized ferrocene-based bis-imidazolium salts **77a–c** and ferrocene-based bis-benzimidazolium salts **78a–c** (Fig. 7) in which imidazolium/benzimidazolium moieties were linked (*ortho*, *meta*, and *para*) to a xylene group.[70] The results of CV studies showed that addition of F^- to receptors **77–78** in CH_3CN solutions caused "two-wave behavior" responses, which can be attributed to strong interactions between F^- and the receptor. Moreover, the *meta*-receptor **77b** ($\Delta E_{1/2}$ = −186 mV) exhibits a larger negative potential shift than do the *ortho*-receptor **77a** ($\Delta E_{1/2}$ = −145 mV) and *para*-receptor **73c** ($\Delta E_{1/2}$ = −104 mV). The $\Delta E_{1/2}$ values of **78a–c** were similar to those of **77a–c**. ^{1}H NMR titration experiments clearly demonstrated that all receptors formed 1:1 stoichiometric complexes through $(C–H)^+\cdots X^-$ hydrogen bonding.

Ding and co-workers reported the results of studies using a new cationic dansyl derivative-based (DIlSD) fluorescent probe **79** (Fig. 8).[71] This ternary sensor system was prepared by combining the fluorophore with anionic surfactant assemblies and Cu^{2+}. The optimized composition was determined to be 4 mM SDS and 25 μm Cu^{2+} on the basis of results arising from various photophysical studies. This DIlSD/SDS/Cu^{2+} sensor system displayed arginine (Arg) induced fluorescence quenching. The Stern–Volmer quenching constant was determined to be 1.34 × 10^5 M^{-1}, and the detection limit was as low as 170 nM. In contrast, 11 other amino acids do not produce significant fluorescence changes. The imidazolium group in DIlSD played an essential role by allowing the fluorophore to both electrostatically interact with SDS assemblies and bind with Cu^{2+} through the N atom that was connected to the methyl group.

3.2 Polyimidazolium receptors

Yoon and co-workers developed the novel receptor **80** (Fig. 9), which has four imidazolium and pyrene groups.[72] The receptor displayed a selective and large fluorescence quenching effect

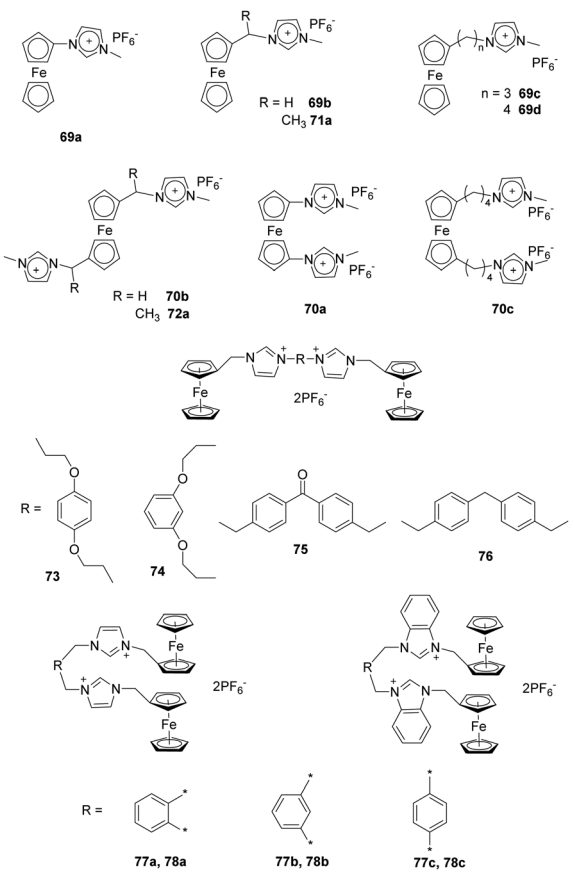

Fig. 7 Structures of compounds **69–78**.

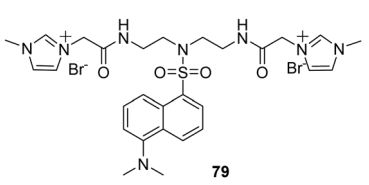

Fig. 8 Structure of compound **79**.

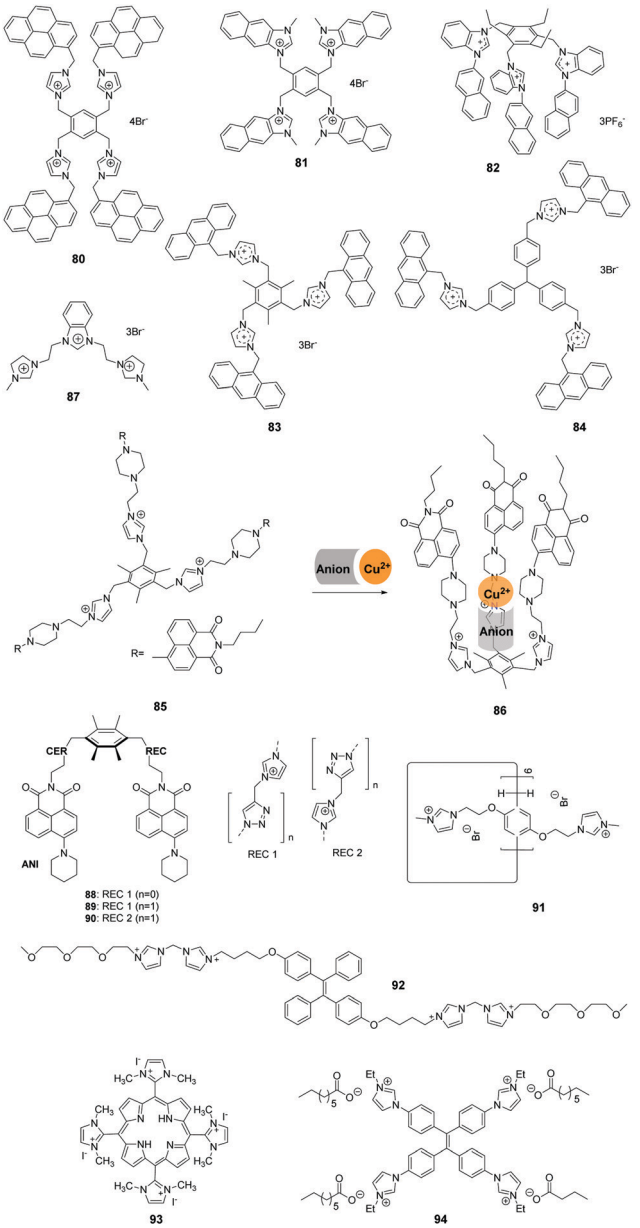

Fig. 9 Structure of compounds **80–94**.

with D-*myo*-inositol 1,4,5-trisphosphate (*myo*-IP_3) (K_a = 1.6 × 10^5 M^{-1}) among other inositol phosphate (IP) series members (IP_1, IP_2, IP_3, IP_4, IP_5, IP_6 and *scyllo*-IP_3), pyrophosphate, and ATP. Notably, the binding of **80** with IP_3 resulted in the separation of the two pyrene moieties, which induced a dramatic decrease in excimer emission at 486 nm. The selectivity and sensitivity of **80** were ascertained using ^{1}H NMR, UV-vis and fluorescence spectroscopic methods.

Continuing their work on polyimidazolium receptors, Yoon and co-workers replaced the imidazolylmethyl pyrene group in **80** with naphthoimidazolium moieties to create the new tetranaphthoimidazolium receptor **81** (Fig. 9).[73] This sensor displayed selective fluorescence enhancement in the presence of phytate in 100% aqueous solution at pH 7.4. The excimer emission at 465 nm increased linearly in the range of 300 nM to 1 mM with a detection limit of 2.28 × 10^{-7} M^{-1}. ^{1}H NMR analysis, density functional theory (DFT) and time-dependent DFT were used to obtain insight into the binding modes and fluorescence behaviors of the probe.

Kumar and co-workers developed a 1-(2-naphthyl)benzimidazolium-based tripod sensor **82** (Fig. 9) that exhibited highly selective fluorescence enhancement in the presence of surfactants sodium dodecyl benzenesulfonate (SDBS) and SDS in a 95% aqueous medium (5% DMSO).[74] Addition of SDBS and SDS to solutions of **82** resulted in a large fluorescence enhancement along with a hypochromatic shift from 450 nm to 415 nm. An analysis of the Job plots showed that 1 : 1 stoichiometric complexes of TRI-BINAP-1 with SDBS and SDS were formed. ^{1}H NMR data and theoretical calculations showed that strong binding occurs between three imidazolium C–H protons and the three oxygen atoms of the surfactant anion. Also, hydrophobic interactions take place between the naphthyl rings and aryl or alkyl protons in the surfactant molecules. The association constants (log β) towards SDBS and SDS were calculated to be 5.75 ± 0.09 and 5.41 ± 0.08, respectively, using fluorescence titration.

Mukherjee and co-workers described two tris-imidazolium salt based probes **83** and **84** that serve as selective sensors for picric acid (PA) in both organic and aqueous media (Fig. 9).[75] The fluorescence intensities of sensors **83** and **84** displayed large decreases upon addition of increasing amounts of PA, which are due to deprotonation induced by the picrate ion. Theoretical studies showed that unusual ground-state electron transfer occurs from the picrate anion to the sensor molecules. The Stern–Volmer constants were calculated to be 3.8 × 10^4 M^{-1} and 3.3 × 10^4 M^{-1} for sensors **83** and **84**, respectively. The results of X-ray diffraction and ^{1}H NMR studies confirmed that 1 : 2 molar complexes form between sensors **83** and **84** and PA.

Zhao and co-workers designed the preorganized tripodal receptor **85** (Fig. 9), which incorporates imidazolium and 1,8-naphthalimide dye moieties.[76] The addition of $Cu(ClO_4)_2$ and $Cu(NO_3)_2$ induced selective "turn on" fluorescence responses with blue-shifted emission from 518 nm to 496 nm, accompanied by a significant color change from yellow-green to bright blue, due to the coordination effect and anion-induced conformational change. No marked fluorescence enhancement of **85** was observed in the presence of other metal salts under the same conditions. The fluorescence blue-shift was caused by ICT, and the enhancement was ascribed to the PET mechanism. Mass spectrometric and NMR spectroscopic titration studies demonstrated that this receptor formed 1 : 1 host–guest complexes **86** with $Cu(ClO_4)_2$ and $Cu(NO_3)_2$.

Singh and co-workers described a benzimidazolium- and imidazolium-based trication probe **87** (Fig. 9) that contains acidic hydrogens that participate in hydrogen bonding.[77] This trication was shown to interact selectively with cysteine (Cys) over other thiols and various anions in water. The specific response towards Cys compared to other analytes was caused by differences in hydrogen bonding of **87** with Cys. The detection

limit for **87** towards Cys was calculated to be as low as 48 nM. By examining the results of spike/recovery assays, the recovery of added Cys in **87** was in the range of 99.6–100.5, which indicated that this probe can be used for measuring Cys in a real biological system (such as human serum) without interference.

Aminonaphthalimide-based two-armed fluorescent imidazolium/triazole receptors **88–90** (Fig. 9) were synthesized by Bitter and co-workers.[78] The receptors were designed to detect nucleoside polyphosphates selectively based on their heterocyclic groups. Receptor **90** was created by inverting the imidazolium and triazole units in the binding site of **89**, which formed much stronger 1 : 2 complexes with ATP, GTP and UTP and showed high selectivity over di-and monophosphates. The association constants ($\log K$) of **90** were calculated to be 6.38 ± 0.05, 6.5 ± 0.3, and 6.37 ± 0.06 for ATP, GTP and UTP.

Xue and co-workers prepared silver nanoparticles by utilization of a water-soluble pillar[6]arene **91** (Fig. 9) containing 12 imidazolium groups. These stabilized silver nanoparticles served as colorimetric probes to selectively detect glutamic acid (Glu).[79] The addition of Glu induced aggregation of the silver nanoparticles in aqueous solutions, which was accompanied by a red-shift in the absorbance spectrum from 400 nm to 500 nm and broadening of the surface plasmon resonance band. X-ray diffraction and transmission electron microscopy were employed to gain an understanding of this phenomenon. The limit of detection for Glu was reported to be 2.8×10^{-6} M.

The bis-imidazolium group (BIM) is reported to bind with adenosine-5′-triphosphate (ATP) selectively and efficiently. Recently, Li and co-workers synthesized the water-soluble fluorophore **92** (Fig. 9), in which a BIM group and oligo-(ethylene glycol) (EG) moieties modify the TPE core. ATP-induced self-assembly of **92** in aqueous solution was then used to prepare fluorescent organic nanoparticles.[80] The nanoparticles displayed a remarkable fluorescence enhancement up to 20-fold due to the existence of strong electrostatic attractions and π–π stacking. Fe^{3+} ions specifically quenched the fluorescence of the nanoparticles by coordination with the imidazolium moieties. The relationship between the fluorescence intensity and Fe^{3+} concentration displayed good linearity in the range of 1–10 nM, which allowed **92** to be employed for bioimaging.

Oliveira and co-workers reported multifunctional luminescent nanomaterials by doping mesoporous silica SBA-16 with a cationic porphyrin bearing imidazolium substituents (**93**) to detect toxic Cu^{2+}, Pb^{2+} and Hg^{2+} ions.[81] Probe **93** was colorimetrically selective for Cu^{2+}, Pb^{2+} and Hg^{2+}, presenting distinct colors (pink for Cu^{2+}, green for Pb^{2+} and brown for Hg^{2+}), followed by quenching of the emission intensity of the two bands centered at 635 and 702 nm in the presence of these metal ions. The minimum concentrations observed by absorption at 540 nm (Cu^{2+}), 590 nm (Pb^{2+}) and 575 nm (Hg^{2+}) were 5.8 ppm, 3.8 ppm and 3.6 ppm, respectively. The solid-state SBA-16@**93** showed the same colorimetric/fluorometric responses for metal ions. Moreover, the SBA-16@**93** mesoporous nano system provided a naked eye detection limit of 5 ppm for both metal ions and a minimal detectable amount of 2 ppb (maximum allowed in drinkable water) for Hg^{2+} ions.

Vesicles have been used in drug/gene delivery and artificial bioreactors for biological membranes. Wang and co-workers developed imidazolium salts with multiple imidazolium moieties and alkyl carboxylate counter anions to construct counterion-induced vesicles in aqueous media.[82] The counter anion was the key to triggering vesicle formation, and the introduction of AIEgen TPE as the core of the imidazolium salt **94** induced the formation of functional fluorescent vesicles. This functional imidazolium salt **94** penetrated the cell membranes and exhibited highly specific nucleus imaging with bright blue emission in living cells. The aggregation-induced strong fluorescence emission of **94** may be the main reason for the specific fluorescence images of the cell nucleus.

3.3 Chiral receptors

1,1′-Binaphthyl-based (BINOL) cyclic and acyclic imidazolium chemosensors **95–99** (Fig. 10) have been employed by Lan and co-workers for selective recognition of tryptophan (Trp) among other α-amino acids.[83] The cleft-like receptor **95** exhibits more significant affinity and selectivity towards L-Trp than do **96–99**, as reflected in the association constants of **95**, **96**, **97**, **98** and **99** of 1.73×10^4, 8.04×10, 2.89×10^3, 4.78×10^3 and $2.59 \times$

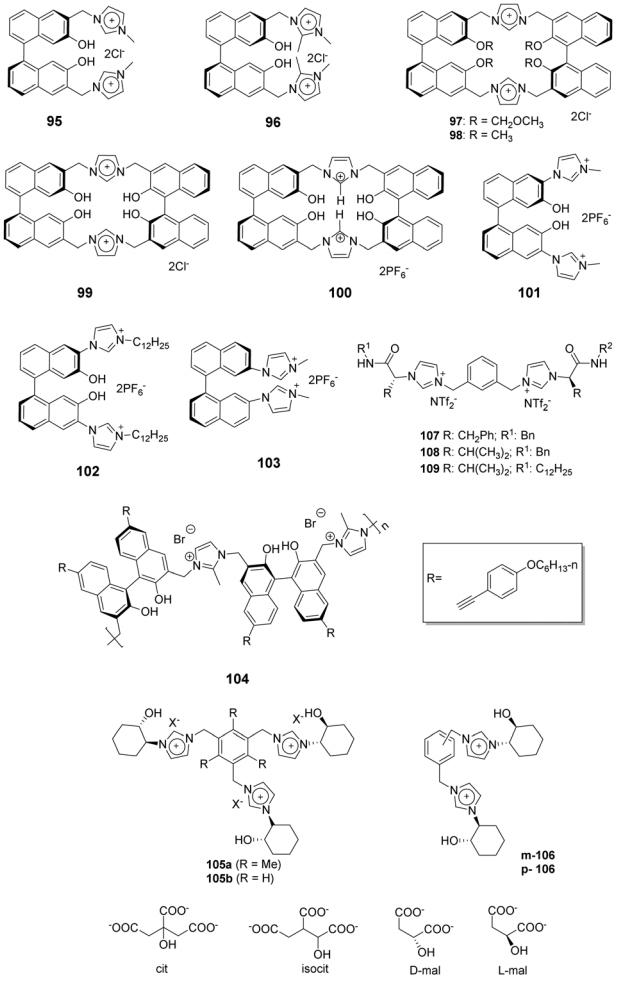

Fig. 10 Structures of compounds **95–109**.

10^3 M^{-1}, respectively. Receptor **96**, which lacks the C-2 hydrogen of the imidazolium nucleus, showed small changes upon addition of various amino acids. This observation demonstrated that the C-2 hydrogen atom of the imidazolium ring plays a vital role as a hydrogen bond donor. Due to a reduced cavity size that leads to a better guest fit, the macrocyclic system **97** displays remarkable enanti-discrimination for tryptophan with K_D/K_L values as high as 6.2.

Yu and co-workers described a BINOL imidazolium cyclophane **100** (Fig. 10) that contains an acidic tetrahydroxy moiety as a multifunctional receptor.[84] Among various anions, F^- in acetonitrile induces a significant increase in the I_{458}/I_{370} ratio as well as a bathochromic shift. ^{1}H NMR titration studies show that the imidazolium C_2–H displays a distinct downfield shift upon addition of F^-. Probe **100** also shows moderate selectivity for L-Boc-phenylalanine over its (D)-isomer. The association constants for the tetrabutylammonium salts of *t*-Boc-L-phenylalanine and of *t*-Boc-D-phenylalanine were calculated using data gained in fluorescence titration experiments and were 43 000 M^{-1} and 64 200 M^{-1}, respectively.

The same group also applied BINOL derivatives conjugated with bisimidazolium to create effective anion probes **101–102** (Fig. 10).[85] The fluorescence of receptor **101** exhibits a dramatic bathochromic shift upon addition of F^- (λ_{max} = 474 nm) and AcO^- (λ_{max} = 454 nm) in CH_3CN/DMSO (v:v = 9 : 1). In addition, a colorless solution of **101** turns a deep yellow after addition of F^-, while a pale yellow color is induced by AcO^-. The fluorescence of probe **102**, which contains a lipophilic dodecyl appendage at the imidazolium nitrogen, exhibits a distinct enhancement upon interacting with anions as compared with that of **101**. This observation demonstrates that the length of the paraffin chain causes a change in the intramolecular charge-transfer (ICT) behavior. The BINOL skeleton also serves as the basis for the ability of **101** and **102** to display enantioselectivity K_L/K_D = 4.5 for **101** and 4.1 for **102** in binding the *t*-Boc alanine anion.

Bisimidazolium has been joined to a binaphthyl moiety to create a substance for chiral recognition **103** (Fig. 10) by Yoon and co-workers.[86] Host **103** displayed chelation enhanced quenching effects in the presence of (*S*)-2-phenylbutylate and (*R*)-2-phenylbutylate, which was due to the PET process. The chiral selectivity was investigated using isothermal titration calorimetry (ITC) methods and fluorescence and ^{1}H NMR spectroscopy.

Zhu and co-workers designed a novel ionic polymer **104** incorporating a chiral BINOL center and imidazolium cations as repeating units.[87] This polymer exhibited high enantio selectivity and sensitivity in response to α-amino acid anions in a wide range of concentrations. This was especially true for the detection of PG-TBA and Phe-TBA, where ef (enantiomeric fluorescence difference ratio) values as high as 14.07 and 12.37, respectively, were observed. The results of fluorescence titration and circular dichroism (CD) experiments provided information about the chiral recognition mechanism. Additionally, the color change of **104** in THF to bright green was observable by the naked eye after addition of (L)-α-amino acid anions.

Alfonso and co-workers synthesized the bi- and tri-podal imidazolium compounds **105** and **106** (Fig. 10) by linking enantiopure (*S*,*S*)-2-(1-imidazoyl)-cyclohexanol to a central aromatic spacer.[88] The tripodal receptor **105** has a cone-type conformation containing an anion binding site surrounded by three imidazolium arms. In contrast, the bipodal receptor **106** has an extended and open conformation. The results of ^{1}H NMR titration experiments with **106** in CD_3CN : CD_3OH (9 : 1) showed that the probe strongly interacts with dianionic malate (K_a = (1.7 ± 0.3) × 10^4 M^{-1}). This interaction was stronger than with trianionic citrate (K_a = (4.9 ± 0.5) × 10^3 M^{-1}) or isocitrate (K_a = (3.9 ± 0.5) × 10^3 M^{-1}). These findings demonstrated that the smaller substrate (malate) fits better in the binding cavity of **106**. The results of theoretical calculations also showed that **106** contains a much more potent cationic and H-binding donor site compared to the analogous bipodal derivatives *m*/*p*-2.

A new family of bis(imidazolium)-based chiral ionic liquids (CILs), *i.e.*, **107–109** in Fig. 10, were reported by Luis and co-workers.[53] The substances, which were synthesized using simple reactions from commercially available amino acids, were used for enantiomeric recognition of dicarboxylic amino acids. ^{1}H NMR titration experiments showed that these substances displayed selectivity towards aspartate that varied in the order **108** > **107** ≈ **109**. They also exhibited enantioselective recognition of L-aspartate over its D-isomer. The binding between the receptors and selected carboxylate substrates was further studied using ^{1}H NMR, NOE and ATR-FTIR.

3.4 Cyclic receptors

In a continuation of earlier work, Beer and co-workers developed a new imidazoliophane probe **110** (Fig. 11) that contains a ferrocene motif at the C_2 position of the imidazolium ring.[89] This substance exists as a 55 : 45 mixture of the *anti* (**110**-*anti*) and *syn* (**111**-*syn*) isomers because of hindered rotation of the internal rings. The anion binding properties of this probe were investigated using ^{1}H NMR spectroscopy and Osteryoung square wave voltammetry (OSWV). The **111**-*syn* isomer displays a high binding affinity towards iodide ions with an association constant of 423(42) M^{-1}. Also, the results of OSWV studies were in accord with the ^{1}H NMR findings. Specifically, the addition of Cl^- induced a ''two wave behavior'' with a more negative cathodic shift (ΔE = −100 mV) than for the Br^- ion (ΔE = −50 mV), whereas the F^- ion did not result in a significant wave change.

Alcalde and co-workers synthesized a family of [1_4]heterophanes containing azolium/azole **112–115** (Fig. 11) using a '3+1' convergent stepwise strategy.[90] A study of the anion binding properties of these substances using ^{1}H NMR titration showed that the charged receptors **112**, **114** and **115** exhibited high affinities for acetate with respective association constants of 10^4 M^{-1}, 5000 M^{-1} and 500 M^{-1}. In contrast, the spectrum of receptor **113** does not change after the addition of acetate. The results confirmed that the imidazolium units in **112**, **114** and **115** exhibited higher affinities for anions than the triazole unit in **113**.

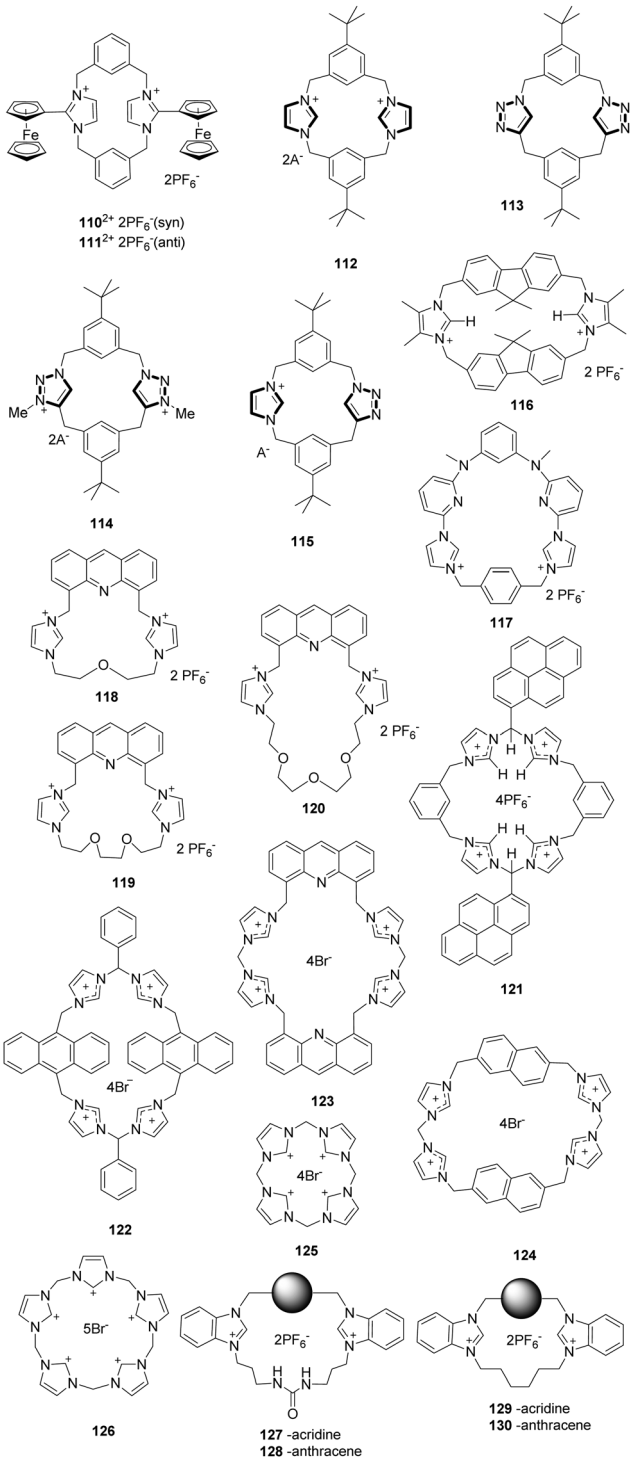

Fig. 11 Structure of compounds **110–130**.

Molina and co-workers reported a ditopicbis(imidazolium) cyclophane receptor **116** for selectively detecting dihydrogen phosphate and hydrogen pyrophosphate anions.[91] The addition of $HP_2O_7^{3-}$ and $H_2PO_4^-$ anions to a solution of receptor **116** induced a remarkable decrease in the intensity of the emission bands (λ = 313, 320 and 338 nm) of the receptor. The interactions between the receptor and these anions were mainly the simultaneous occurrence of O···H–C(sp^3) and O···H–C(sp^2) interactions. Calculations showed that the structures of the complexes were formed with one and two molecules of PF_6^-, $H_2PO_4^-$ and $HP_2O_7^{3-}$, showing that the complexes of the last two anions are more stable than those of PF_6^-.

Gong and co-workers described a pyridine imidazolium-based cationic macrocycle receptor **117** based on an excimer disaggregation induced emission (EDIE) strategy to detect $HP_2O_7^{3-}$ and $H_2PO_4^-$ oxoanions.[92] This macrocycle existed in a supramolecular polymeric form in the solid state based on the X-ray diffraction analyses of single crystals. Receptor **117** displayed little propensity to aggregate in the ground state but formed a poorly fluorescent excimer at [$\mathbf{117}^{2+}$] $\approx$ 0.020 mM in an acetonitrile solution. Addition of $HP_2O_7^{3-}$, $H_2PO_4^-$, and (to a lesser extent) HCO_3^- to **117** (0.020 mM in acetonitrile) resulted in an enhancement in the emission intensity (λ_{ex} = 334 nm; λ_{em} = 390–650 nm), leading to the break up of these aggregated species and the formation of monomeric anion complexes. The single-crystal X-ray diffraction studies obtained after treating **117** with $HP_2O_7^{3-}$ in the presence of water provided support for the proposed EDIE mechanism.

Cyclophane sensors show good performance in recognizing ions due to their pre-organized topology. Lin and co-workers developed a series of cyclophane fluorescent chemosensors **118a–118c** constructed by combining acridine with imidazolium using ether linkages of different lengths.[93] Ether chains of different sizes can be used to modulate the hydrophilicity of the sensor. Their results showed that the hydrogen bond and π–π interactions could drive the self-assembly behavior of these cyclophanes in the solid state *via* X-ray crystal structures analysis. As expected, sensors **118–120** showed specific responses to Fe^{3+} in aqueous solution (H_2O/CH_3CN = 49 : 1, v/v) and $H_2PO_4^-$ in acetonitrile solution with a notable color change under UV light. An apparent fluorescence emission quench was induced by Fe^{3+} in aqueous solution, and an impressive bathochromic-shift was induced by $H_2PO_4^-$ in acetonitrile solution. Interestingly, the bathochromic shifts induced by $H_2PO_4^-$ were distinctly different for the different sensors, 77 nm for **118**, 81 nm for **119** and 70 nm for **120**.

Kim and co-workers synthesized the imidazolium-based cyclophane **121** (Fig. 11), which served as a selective fluorescent chemosensor for I^-.[94] In CH_3CN–HEPES (9 : 1, 20 mM HEPES buffer, pH 7), cyclophane **121** displayed monomer emission at 381 nm and excimer emission at 472 nm. Among various anions, I^- induced a selective fluorescence quenching effect for both the monomer and excimer emission. It was found that cyclophane **121** binds to I^- with a stoichiometry of 1 : 2. The results of NMR experiments and theoretical calculations suggested that imidazolium $(C–H)^+\cdots I^-$ ionic hydrogen bonding and bridged methine C–H···I^- hydrogen bonding interactions were responsible for the selectivity of I^-.

In a continuation of this work, Kim and co-workers designed three different imidazolium-based cyclophanes **122–124** (Fig. 11) in which different fluorophores are bridged by spacer groups.[95] The anthracene-based probe **122** in HEPES buffer at pH 7.4 undergoes the largest decrease in excimer fluorescence at

495 nm in the presence of AMP in comparison to other nucleosides such as ADP and ATP. This change was attributed to the H–π interactions between the anthracene moieties in **122** and the adenine moiety of AMP. Probe **123** displayed almost 87% fluorescence quenching upon addition of GTP due to the presence of ionic interactions. In the case of **124**, an intermolecular π–π interaction with pyrophosphate (PPi) in aqueous solution resulted in the formation of a unique excimer peak at 407 nm.

Receptors with an array of imidazolium moieties in a calix form have been widely used for anion sensing because their binding affinity can be regulated by adjusting the cavity size. Kim's group synthesized the imidazole-based homo-calix compounds **125** and **126** (Fig. 11).[96] The quadruple-charged receptor **125** displayed excellent binding to F^- in water with a large binding constant of 8.3×10^4 M^{-1}. A 1:1 binding stoichiometry between F^- and **125** was confirmed using isothermal titration calorimetry and DFT calculations. The calculations also showed that the quadruple-charged receptor **125** can be used to recognize neutral fullerenes through π^+–π interactions.

Gao and co-workers prepared four macrocyclic fluorescent compounds **127** to **130** (Fig. 11), in which benzimidazolium and urea groups act as cooperative anion binding sites, while acridine or anthracene act as fluorophores.[97] In CH_3CN, these compounds displayed selective ratiometric fluorescence changes upon the addition of $H_2PO_4^-$. For example, the emission at 501 nm increases with a concomitant decrease of the emission at 430 nm when $H_2PO_4^-$ is added to solutions of **127** or **128**. The band at 501 nm was attributed to excimer emission. The association constants of **127**, **129** and **130** with $H_2PO_4^-$ were calculated to be 2.9×10^6, 2.6×10^5 and 1.6×10^6 M^{-1}, respectively.

Sessler and co-workers described neutral and anionic guest recognition by the large, cationic tetraimidazolium receptor **131** (Fig. 11).[98] The interactions of receptor **131** with different anions were probed using NMR and X-ray methods. First, **131** formed a 1:1 pseudorotaxane complex with the dianion of 2,6-naphthalene dicarboxylic acid. Cl^- directly replaced the 2,6-naphthalene dianion from the preformed complex. In this process, Cl^- initially forms a 1:1 complex with **131**, which was then followed by subsequent formation of a 1:2 complex. In contrast, the addition of NO_3^- caused displacement of naphthalene dicarboxylate by a stepwise process for stabilizing an outside binding mode under appropriate conditions. Additionally, when biphenyl-3,4,3′,4′-tetraamine was added as the guest to **131**, a stable 1D-donor–acceptor–donor coordination-based polymer was generated.

Because the tetracationic macrocycle **131** has the ability to have disparate supermolecular structures, Sessler and co-workers questioned whether structurally related macrocyclic systems might display similarly recognition chemistry. To answer this question, they designed three new tetracationic macrocycles **132–134** (Fig. 11).[99] These imidazolium containing receptors were also found to bind 2,6-naphthalenedicarboxylate dianions in solution and the solid state. However, solid state binding occurred with distinctly different stoichiometries as determined using single-crystal X-ray analysis. Binding of **132** with the 2,6-naphthalenedicarboxylate dianion *via* an "outside" binding mode formed a 1:1 complex ($K_a = 2.3 \pm 0.1 \times 10^4$ M^{-1}). In contrast, binding of this dianion with **133** occurs by an "insert" 1:1 binding mode ($K_a = 3.2 \pm 0.1 \times 10^4$ M^{-1}), while **133** was observed to form a 2:3 complex with this dianion *via* "outside binding" ($K_a = 7.3 \pm 0.2 \times 10^6$ M^{-1}). These observations demonstrated that the members of this new class of receptors have high inherent flexibility, which enabled them to adopt multiple stable conformations.

Recently, the same group applied a post-synthetic modification (PSM) approach to prepare novel macrocyclic receptors. Under mild basic conditions, ring-opening of the imidazolium moieties in **132** occurs to produce "*cis*" (**135**) and "*trans*" (**136**) constitutional isomers (Fig. 12) in relatively high yields (86–93%).[100] The results of NOESY and 1D NOE spectroscopic studies showed that macrocycles **135** and **136** undergo rapid interconversion. Also, single crystal X-ray analysis showed that **135** exists in two conformations in the solid state, an observation that is consistent with the relative flexibility of this ring-opened receptor. Furthermore, ESI-MS analysis results revealed that **135** and **136** displayed outside binding or weak ion pairing with dianionic substrates.

The bis-cationic macrocycles **137–140** (Fig. 12), containing imidazolylboronium ions, were synthesized by Parrain and co-workers.[101] In these substances, 9-borabicyclo[3.3.1]-nonane (9-BBN) moieties were connected to bis-imidazolylaryl groups to form rigid and well-defined imidazolylboronium macrocycles. X-ray crystal structure analysis, mass spectrometry (MS) and various NMR methods were used to gain information about the unique binding properties of these substances towards anions. For example, the NMR titration results showed that the respective association constants for macrocycle **140** for Cl^- and F^- were 4.06×10^3 M^{-1} and 3.96×10^3 M^{-1} in DMSO. Multiple C_{sp^2}–H and unusual C_{sp^3}–H hydrogen-bonding donors in these receptors played critical roles in the recognition of anions. Interestingly, positive-mode ESI-MS studies were employed to show that **140** can detect anion concentrations below 0.1 μM. This receptor was used to detect NO_3^{2-} in commercial sparkling mineral water.

Beer and co-workers developed the highly stable tetracationic imidazoliophane **141** (Fig. 12), which displays high affinities towards π-electron rich neutral guests.[102] ^1H NMR titration studies showed that addition of 1,5-dihydroxynaphthalene to **141** in CD_3CN results in a significant upfield shift of the macrocycle phenylene (Ha) proton ($\Delta\delta_{10equiv.} = -0.477$ ppm). The results of a crystallographic investigation demonstrated that **141** formed an inclusion complex with an association constant of 1880 M^{-1}. The anion binding properties of **141** were probed using NMR spectroscopy and were found to be dependent on the basicity and size of the anion in the order $Cl^- > Br^- > I^-$.

You and co-workers described the rigid tetrakisimidazolium macrocycle **142** (Fig. 12), which displayed highly selective fluorescence recognition of sulfate dianions in water.[103] The results of fluorescence studies revealed that **142** and sulfate

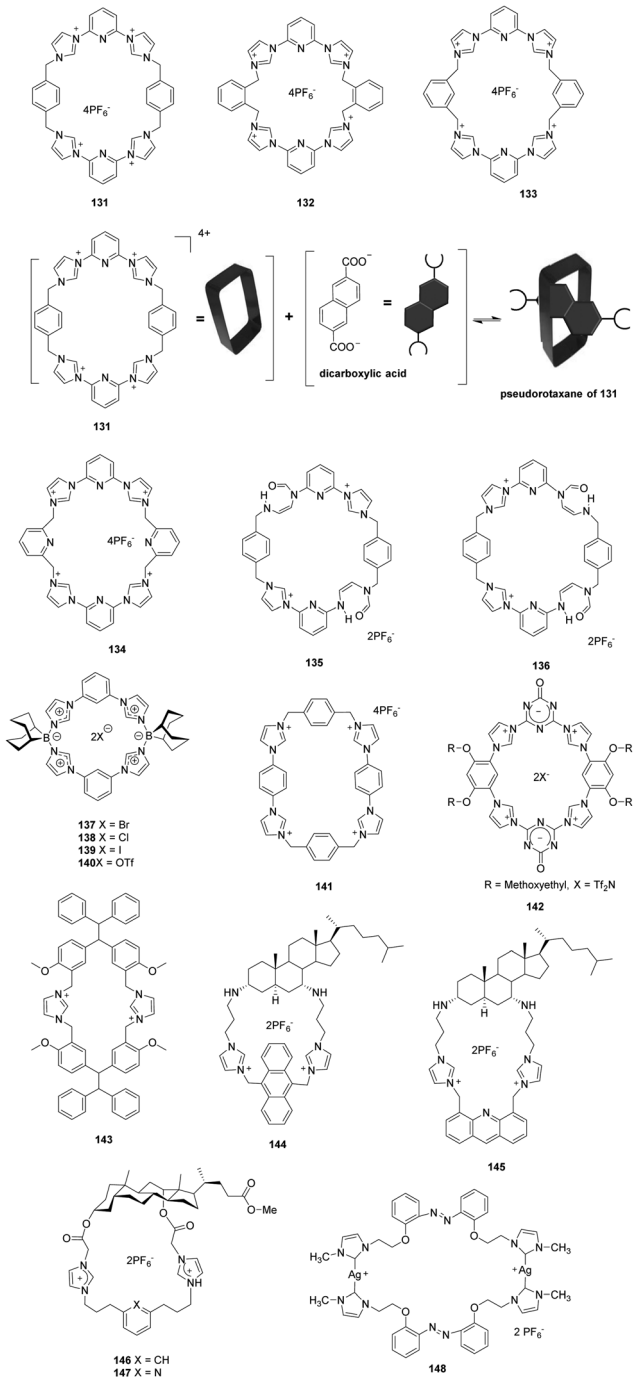

Fig. 12 Structure of compounds **131–148**.

dianions form a 2 : 1 complex with a high binding affinity (K_a = 8.6 × 10^9 M^{-2}). Further anion binding studies were carried out using XRD and single crystal X-ray analysis. The results of this effort indicated that sulfate is encapsulated in a pseudo-hexahedral cavity of the sandwich structure created by two orthogonally packed rigid macrocyclic rings in **142**. The presence of π–π stacking and peripheral-backbone hydrogen protection prevented sulfate from interacting with the solvent.

Zheng and co-workers synthesized the imidazolium macrocycle **143** (Fig. 12), which contains a TPE group.[104] This TPE derivative does not undergo a fluorescence change upon addition of pyrophosphate anions (PPi). In contrast, **143** does interact with PPi to form a complex that exhibits strong fluorescence in the presence of zinc cations. This phenomenon was attributed to aggregation created by coordination of the complex with zinc. The association constant of **143** with pyrophosphate was 1.41 ± 0.10 × 10^4 M^{-1} as determined using by a UV-vis titration method.

Kim and co-workers reported the imidazolium functionalized cholestane derivative **144** (Fig. 12), in which an anthracene group is connected to imidazolium *via* its 1,8-positions.[105] Upon excitation at 374 nm, typical anthracene emission bands were seen at 402, 426 and 451 nm. In dry acetonitrile, **144** displayed a high binding constant (1.6 × 10^5 M^{-1}) with $H_2PO_4^-$ among various other simple anions. Addition of $H_2PO_4^-$ caused selective and large fluorescence quenching (about 95%) due to a PET process. The authors pointed out that the acidic C–H imidazolium proton and two N–H protons in the 3,7-diamine group serve as hydrogen bonding donors and form an excellent binding pocket composed of anthracene and cholestane backbones.

The same group showed that the acridine-imidazolium cholestane derivative **145** (Fig. 12) serves as a fluorescent chemosensor for $HP_2O_7^{3-}$ (PPi).[106] About 70% quenching of the fluorescence of **145**, occurring *via* a PET mechanism, is promoted by $H_2PO_4^-$ (Pi) and $HP_2O_7^{3-}$ (PPi) among other anions in dry CH_3CN. The association constant of **145** with PPi was calculated to be 1.5 × 10^4 M^{-1}.

Bile acid derivatives **146–147** (Fig. 12), in which two imidazolium and amide groups act as hydrogen bond donors, were synthesized by Pandy and co-workers.[107] In contrast to various anions such as F^-, Cl^-, Br^-, AcO^- and $H_2PO_4^-$, only HSO_4^- induces gel formation of **146–147**. Addition of HSO_4^- produced an upfield shift of the aryl-CH and amide-NH peaks in the NMR spectrum of **146**, and the peaks disappeared after addition of 0.9 equiv. HSO_4^- due to gel formation.

Wei and co-workers synthesized and characterized a bis-imidazolium salt 2,2′-di[2″-(*N*-methyl-imidazoliumyl)ethoxyl]-azobenzenehexafluorophosphate and its macrometallocycle binuclear N-heterocyclic carbene silver(I) complex with bridging azobenzene **148**.[108] X-ray single crystal diffraction showed that one 34-membered macrometallocycle was formed by two biscarbene ligands and two silver(I) ions in complex **148**. In addition, **148** had special selectivity for detecting HSO_4^- based on an increase in fluorescence intensity at 363 nm. The association constant K was calculated to be 4.19 × 10^{11} M^{-1} (R = 0.997) from fluorescence titration, and K_S was calculated to be 1.13 × 10^{11} M^{-2} from UV/vis titration for **148**·HSO_4^- using a 1 : 2 association equation analysis. The detection of HSO_4^- using **148** was highly sensitive, and the detection limit was estimated to be 7.5 × 10^{-9} mol L^{-1}.

3.5 Caged receptors

Yoon and co-workers synthesized two extremely rigid cage compounds, **149** and **152** (Fig. 13), which contain three imidazolium groups inserted between two substituted benzene rings.[109] The cyclophane cavities bridged with three naphthoimidazolium

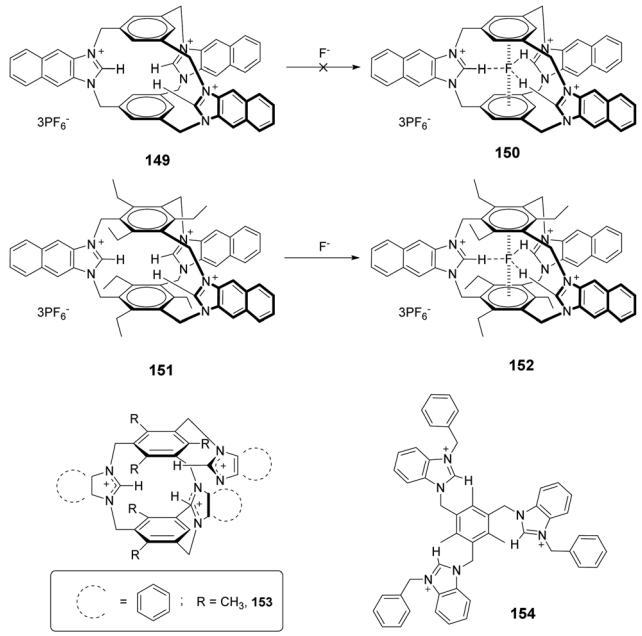

Fig. 13 Structure of compounds **149–154**.

groups in these substances cause selective complexation with fluoride ions through anion–π and $(C–H)^+\cdots$F-type ionic hydrogen bonding interactions. ^{1}H NMR, ^{19}F NMR and fluorescence spectroscopic methods were used to examine the interactions of fluoride ions with **149** and **151**. The results showed that only **151** hosts a fluoride ion in the cavity between two alkylbenzene rings forming a sandwich complex. The difference is attributed to the stronger anion–π interactions between F^- and the triethyl benzene moiety. The results of fluorescence titration experiments showed that F^- results in a dramatic increase in the emission intensity of **151** at 385 nm, whereas a significant decrease in the intensity of the band at 474 nm occurs. Using isothermal titration calorimetry (ITC), these workers showed that the Gibbs free energies ($-\Delta G$) for **149** and **151** complexed with F^- are 6.07 kcal mol^{-1} and 7.94 kcal mol^{-1}, respectively.

Fusco and co-workers described imidazolium-based cage hosts **153–154** (Fig. 13).[110] They showed that the trisbenzimidazolium cyclophane receptor **151** has a high affinity towards F^- anions. Geometric considerations suggested that fluoride is present in the middle of the equilateral 3C triangle (three imidazolium carbon atoms) as a result of the presence of three C–H$\cdots$FH-bonds. The trisbenzimidazolium tripodal receptor **154** does not provide size exclusion selectivity, and, as a result, forms a 1 : 1 complex both with F^- and with Br^- and the polyatomic anion NO_3^-. In these cases, the anions were located below the 3C triangle due to the steric restraints. The $[\mathbf{154}\cdots F]^{2+}$ complex ($\log K > 7$) is more stable than the $[\mathbf{154}\cdots F]^{2+}$ tripodal complex ($\log K = 5.75$), which was likely ascribable to the high degree of preorganization of **153**. In addition, the cage complex $[\mathbf{153}\cdots F]^{2+}$ was stable in the presence of excess F^-, whereas the tripodal complex $[\mathbf{154}\cdots F]^{2+}$ decomposed due to deprotonation of an imidazolium C–H fragment.

3.6 Polymer receptors

Yoon and co-workers prepared a new type of polydiacetylene (PDA) **155** (Fig. 14) that contains an imidazolium head group for detection of cationic surfactants.[111] **155** exhibits selective and unique color and fluorescence changes in the presence of anionic surfactants. More importantly, SDS and SDBS can be discriminated by the naked eye using this sensor. Specifically, SDS induced a color change in **155** from blue to yellow, while SDBS induced a color change from blue to red. Using fluorescence titration methods, the detection limit for SDS was calculated to be 2×10^{-7} M. Yoon and co-workers utilized the same PDA system to colorimetrically discriminate oleic acid from stearic acid and elaidic acid.[112] **155** undergoes a blue to violet color transition in the presence of oleic acid. On the other hand, it does not undergo a significant color change when treated with stearic acid and elaidic acid.

Yoon and co-workers also designed a new PDA **156** that is functionalized with amines and imidazolium groups (Fig. 15).[113] In this work, **156** was utilized as a colorimetric and fluorescence turn-on sensor for CO_2 detection. The change caused by CO_2 is due to the formation of carbamate anions by the reaction between imidazolium cations with primary amines and CO_2 in the presence of an external base. The resulting partial neutralization of the positive charges induced the blue to red color transition of **156**. UV-vis and fluorescence spectroscopic analyses were employed to analyze the CO_2-induced phase transition of **156**. Furthermore, a solid-state system consisting of electrospun fibers of this PDA can be used to detect CO_2 using the naked eye.

Yoon and co-workers described a rapid and efficient method for detecting and killing bacterial cells, which relies on the use of the imidazolium-conjugated polydiacetylene **157** (Fig. 16).[114] A conventional agar plate counting method was used to investigate the antibacterial efficacy of **157**. It was found that

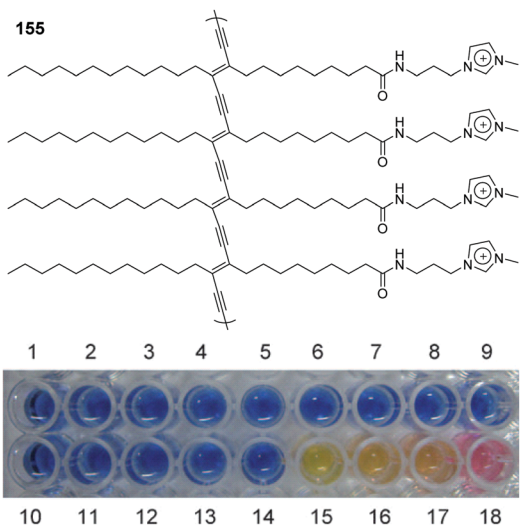

Fig. 14 Structure of polymerized **155**, and colorimetric responses of polymerized **155** (100 mm) in the presence of various analytes (500 μm) in HEPES buffer (20 mm, pH 7.4): 1 blank, 2 F^-, 3 Cl^-, 4 Br^-, 5 I^-, 6 SO_4^{2-}, 7 CO_3^{2-}, 8 ClO_4^-, 9 CH_3COO^-, 10 NO_3^-, 11 HPO_4^{2-}, 12 SCN^-, 13 CTAC, 14 Triton X-100, 15 SDS, 16 SDC, 17 SDP, 18 SDBS.

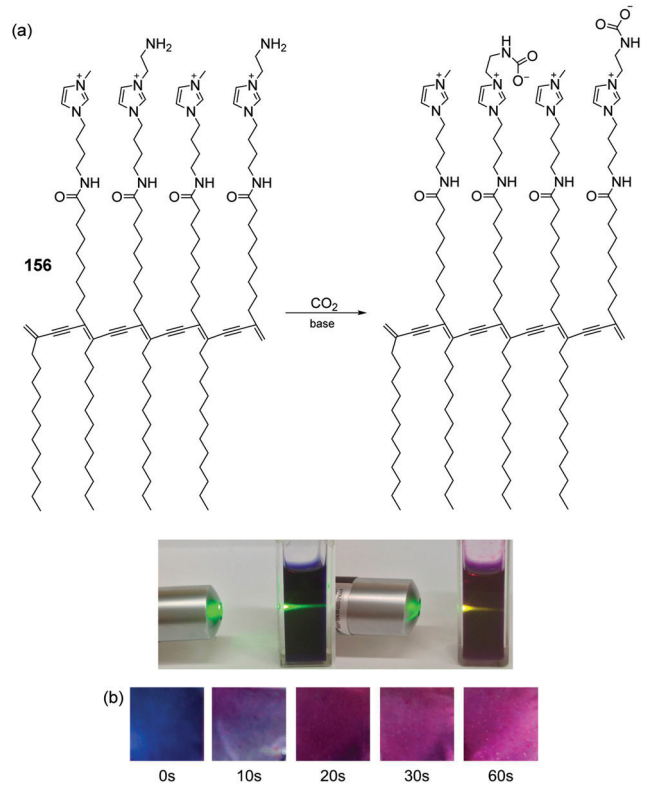

Fig. 15 (a) Structure of **156**, and proposed origin of the CO_2 induced color change. (b) Time-dependent color changes of **156** embedded electrospun microfibers in a CO_2 atmosphere in the presence of saturated TEA vapor.

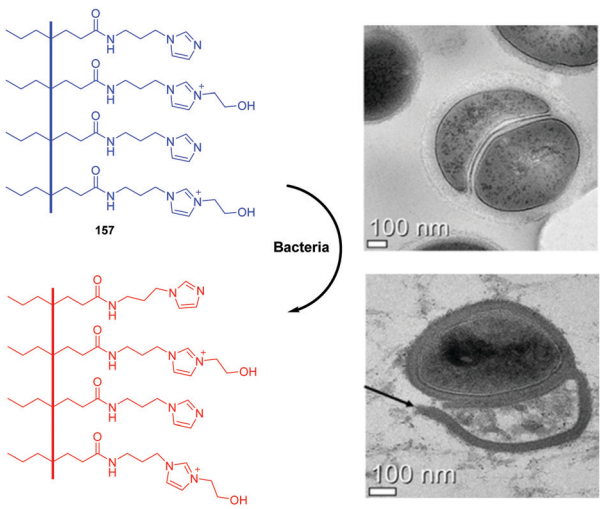

Fig. 16 Structure of **157** and transmission electron microscopy (TEM) images of pathogenic bacteria (*S. aureus*) in the presence and absence of **157**.

Gram-positive bacteria (*S. aureus*, MRSA) are completely killed by this PDA at concentrations below 10 μM, whereas killing Gram-negative pathogens (*E. coli* O157:H7 GFP, ESBL-EC, *S. typhimurium*) requires concentrations of **157** of 100 μM or higher. The results of transmission electron microscopy analysis of bacteria treated with **157** demonstrated that the electrostatic interactions between the negatively charged bacterial cell surface and the positively charged polymers disrupt the cell membrane, which induces bacterial cell death. PDA **157** solution also displayed distinct color and fluorescence changes in the presence of bacterial cells.

Chen and co-workers reported a polydiacetylene-based sensor (**158**) with imidazolium modified heads for detection of phospholipase D (PLD) activity (Fig. 17).[115] PLD plays a crucial role in many biological processes by catalyzing the hydrolysis reaction of a phospholipid to generate phosphatidic acid (PA). Due to the interactions between the imidazolium moieties in PDAs with positive charges and the hydrolysis products (with negative charges), **158** underwent an obvious blue-to-red color transition as well as fluorescence enhancement at 563 nm. A good linear relationship was obtained in the range of 0–0.008 U mL^{-1} with a detection limit of 0.0006 U mL^{-1} towards PLD. Furthermore, **158** was successful applied onto filter paper strips for practical application for detecting PLD activity.

Huang and co-workers prepared imidazolium-functionalized conjugated polythiophene **159** by Grignard metathesis polymerization, and it showed unique light-activated biocidal activity (Fig. 18).[116] The emission of **159** was red-shifted to 611 nm compared to 570 nm in methanol, which was attributed to the π-stacked interchain aggregates. Similarly, **159** particles showed an average diameter of 6.9 nm in methanol and of 61.5 nm in water by dynamic light scattering, which suggests that it aggregated in water. Further, **159** displayed excellent antibacterial efficacies towards both Gram-positive *Escherichia coli* and Gram-positive *Staphylococcus aureus* bacteria. In addition, **159** was used to selectively image bacteria, and it provided efficient antibacterial

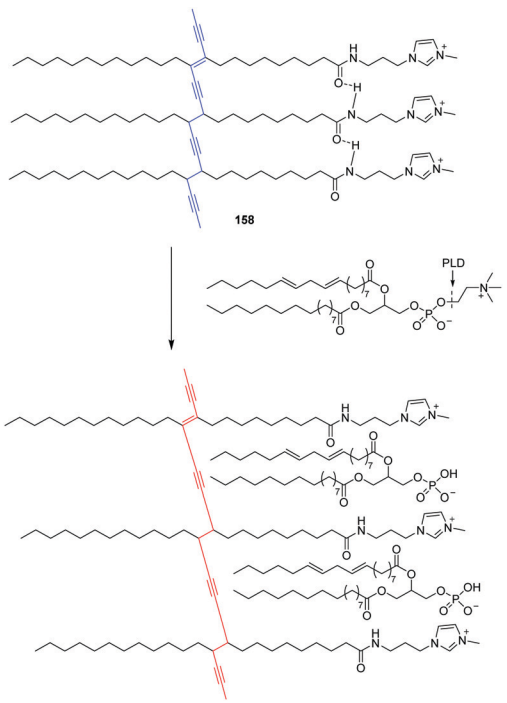

Fig. 17 Mechanism of action of **158** in response to PLD.

Fig. 18 Proposed mechanism of **159** for the selective inactivation of bacteria over mammalian cells.

efficacy over mammalian cells. **159** could kill bacteria even at very low concentrations (<1 μg mL^{-1}) with 1 h visible light exposure. Mammalian cells are almost unaffected under the same conditions. The selective light-activated biocidal activity of **159** was explained by selective binding to the negatively charged bacterial envelope and light-induced bacterial deactivation.

Mao and co-workers described the first example of direct amperometric sensing of electrochemically inactive heparin using polyimidazolium **160** as a synthetic receptor (Fig. 19).[117] The influence of heparin on the stability of the $Fe(CN)_6^{3-}$/**160** nanocomposite was studied using cyclic voltammetry. Addition of **160** to a $Fe(CN)_6^{3-}$ solution results in a decrease in the redox peak current, whereas addition of heparin to this solution leads to an increase in the peak current. This phenomenon demonstrated that anion exchange occurs between $Fe(CN)_6^{3-}$ and heparin due to their different affinities for the synthetic **160** receptor. This amperometric assay was also employed to investigate heparin metabolism in a biological system.

A water-soluble cationic polyelectrolyte (**161**, Fig. 20) containing pendant imidazolium side chain groups was developed by Lyer and co-workers.[118] **161** displayed significant photophysical and conformational changes in the presence of anionic SDBS and SDS at very low levels (31.7 ppb and 17.3 ppb, respectively) over the full pH range of 1–14. The hydrogel formed by drop-wise addition of SDS to **161** displayed extraordinary chemical, thermal and optical stability, whereas the complex **161**/SDBS precipitates because of the different interpolymer co-facial arrangement caused by coulombic attraction. Consequently, the **161** system can be utilized to detect, discriminate and/or eliminate SDS and SDBS from many types of solutions.

Iyer and co-workers also reported a water-soluble cationic conjugated polyelectrolyte **162** based on aggregation-induced fluorescence resonance energy transfer for bacterial imaging (Fig. 21).[119] Cationic imidazolium groups on the polymer side chain provided electrostatic binding sites on the negatively charged bacterial membrane, which resulted in an emission change from blue to bright yellow. Furthermore, **162** exhibited effective antibacterial activity against both *S. aureus* and *E. coli* due to efficient intercalation into the bacterial membrane, which resulted in the disintegration of the membrane and ultimately cell death. The minimum inhibitory concentration (MIC) values for *S. aureus* and *E. coli* were 23.7 and 47.7 μg mL^{-1}, respectively. The stated killing efficacy of **162** was higher for Gram positive bacteria compared to Gram negative bacteria.

Since the bis-imidazolium moiety has a high positive charge density, substances containing this group are good candidates for binding with plasma membranes. Wang and co-workers designed polymer **163** (Fig. 21), which contains a large number of bis-imidazolium groups, as a novel plasma membrane probe.[120] The sidechain of this polymer also possessed olig(ethylene glycol) (EG) moieties, which provide good water-solubility. In cellular imaging experiments, blue channel imaging was first performed by excitation with a 405 nm laser. After 24 h incubation of cells with **163**, an apparent increase in the fluorescence ratio I_{620}/I_{425} occurred in the range of 0.90–1.10. This observation was a result of the enhanced brightness of the red channel. The contrasting intensities of blue and red emission made polymer **163** an ideal staining agent for dual channel cellular imaging.

Zhou and co-workers developed a new class of multifunctional hybrid materials for specific recognition and selective removal of Cu^{2+} in pure aqueous solutions. Specifically, **164** was obtained by anchoring an imidazolium-type crosslinked

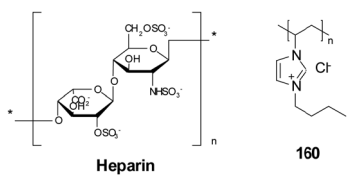

Fig. 19 Structure of **160** and heparin.

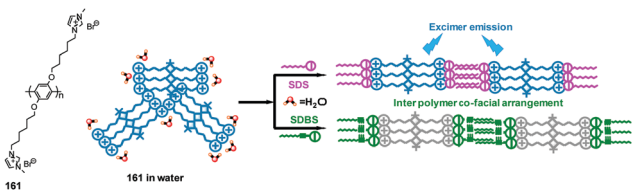

Fig. 20 Structure of **161** and the schematic representation of the aggregation behavior of the **161**–SDS and **161**–SDBS complexes.

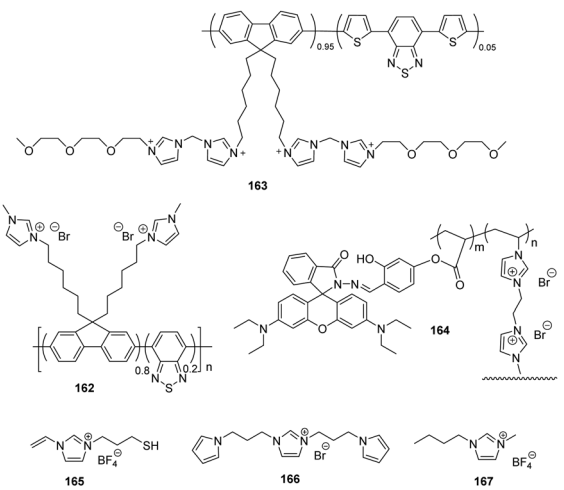

Fig. 21 Structures of compounds **162–167**.

poly(ionic liquid) (CL-PIL) with a rhodamine derivative through free radical copolymerization (Fig. 21).[121] This hybrid material **164** exhibited high hydrophilicity and good dispersibility in pure water due to the positively charged polymeric backbone. Furthermore, **164** exhibited high selectivity and sensitivity towards Cu^{2+} with a significant color change from colorless to pink as observed by the naked eye. The limit of detection (LOD) was calculated to be 0.15 μmol L^{-1}. More interestingly, **164** could be applied as an ideal adsorbent for Cu^{2+} with a high adsorption capacity (19.03 mg g^{-1}) and good reusability in solutions with multiple ions.

An imprinted polymer system made from an electrochemically polymerizing ionic liquid was reported as a neuron specific enolase (NSE) selective sensor by Wang and co-workers (Fig. 21).[122] NSE is known as an important marker for determining the degree of brain damage and for various cancers and diseases, such as small cell lung cancer, and stroke. The detailed procedure of the fabrication of imprinted polymers and the structures of the 1-(3-mercaptopropyl)-3-vinyl-imidazolium tetrafluoroborate **165** and 1,3-di(3-*N*-pyrrolpropyl)imidazolium bromine ionic liquid **166** are provided in Fig. 24. First, gold nanoarrays (GNA) were introduced on a glassy carbon electrode (GCE) surface. Then, **165** containing an active moiety to form an imprinted film was self-assembled on the gold nanoarrays *via* thiol–gold interactions. Electrochemical polymerization was performed in the presence of NSE and **166** followed by removal of the NSE templates. The resulting sensor showed a detection limit of 2.6 pg mL^{-1} for NSE with a linear response range of 0.01 to 1.0 ng mL^{-1}. An imprinted film electrode was further applied to determine the NSE in clinical serum samples with a recovery range between 96.7% and 102.9%. Unfortunately, the roles of imidazoliums were not clearly explained in this paper.

Sun and co-workers utilized graphene quantum dots (GQDs) and 1-butyl-3-methyl imidazolium tetrafluoroborate **167** to form ionic liquid-capped GQDs (IL-GQDs), which were then used as a fluorescent sensor to detect $Fe(CN)_6^{3-}$ (Fig. 21).[123] Strong green emission of the GQDs and IL-GQDs was observed at 512 nm upon excitation at 470 nm. The interactions between **167** and the GQDs were attributed to cation–π interactions and π–π interactions. The addition of $Fe(CN)_6^{3-}$ resulted in a dramatic quenching effect. A detection limit of 40 nM was reported with a linear range of 2.5×10^{-3} to 1.0×10^{-7} M. Among the various anions such as HCO_3^-, $H_2PO_4^-$, $S_2O_8^{2-}$, SCN^-, HPO_4^{2-}, $CH_3CO_2^-$, Cl^-, NO_3^-, S^{2-}, NO_2^-, Br^-, $S_2O_3^{2-}$, $Cr_2O_7^{2-}$, $Fe(CN)_6^{3-}$ and $Fe(CN)_6^{4-}$, the addition of $Fe(CN)_6^{3-}$ and $Fe(CN)_6^{4-}$ resulted in a fluorescence quenching effect of the IL-GQDs. The selectivity was explained by anion exchange between $Fe(CN)_6^{3-}$ and BF_4^- and the selectivity of GQDs for iron based ions.

4. Target anion recognition and sensing

4.1 Phosphate-containing anions

4.1.1 ATP sensing. Duan and co-workers reported two types of chemical sensors that have the potential to distinguish ADP and ATP from other ribonucleotide polyphosphates. The sensors incorporate 1,8-naphthalimide and imidazolium moieties into a preorganized tripodal arrangement.[124] Compound **168** exhibited selective "turn-on" fluorescence when treated with ADP and no other ribonucleotide polyphosphates. Sensor **169** exhibited similar fluorescence responses to ATP, GTP and UTP (Fig. 22). Analysis of the Hill-plot profile of the titration curve suggested a 1 : 2 stoichiometry of the host–guest complexation species, with an association constant $\log K_a$ = 8.75. Fluorescence enhancement of **169** was observed when stained HeLa cells were further incubated with ATP (0.4 mM).

Yoon and co-workers developed a series of anthracene derivatives (Fig. 22) which contain two imidazolium groups at the 1,8- and 9,10-positions. These substances were examined for their fluorescence-based recognition of nucleotides, such as ATP, GTP, CTP, TTP, UTP, ADP and AMP.[125] The anthracene group in these sensors was designed to interact with bases in the nucleotides, and the imidazolium groups induce hydrogen bonding interactions with the phosphate groups. Compound **170** displayed the tightest binding with GTP in association with a fluorescence quenching effect, while a moderate fluorescence enhancement is caused by addition of ATP to this sensor. The association constants for GTP and ATP were calculated to be 8.7×10^4 and 1.5×10^4 M^{-1}, respectively. The fluorescence of the 9,10-isomer **171** was also quenched by GTP, but ATP caused fluorescence quenching in conjunction with a higher association constant. Fluorescence titration was used to show that the association constants of **171** for ATP and GTP are 5.1×10^4 and 2.4×10^4 M^{-1} (errors <10%), respectively.

Yoon and co-workers also reported the synthesis of three naphthoimidazolium derivatives **172–174** and their fluorescence-based recognition of nucleotides in 100% aqueous solutions (Fig. 22).[8] Compound **172** does not undergo significant fluorescence changes in the presence of various anions and nucleotides, such as ATP, GTP, CTP, TTP, UTP, ADP and AMP. On the

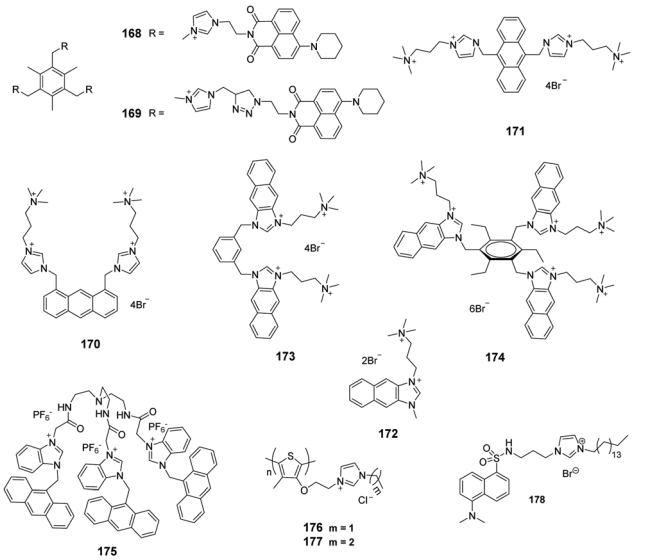

Fig. 22 Structure of compounds **168–178**.

other hand, **174** displayed a large fluorescence enhancement induced by UTP, CTP and TTP, moderate fluorescence enhancements with ATP and pyrophosphate, and fluorescence quenching with GTP. Finally, the dipodal system **173** displays a selective fluorescence enhancement with ATP and a selective fluorescence quenching effect with GTP. The naphthoimidazolium groups in these substances can serve both as a source of ionic hydrogen bonding and of additional interactions with the nucleotide bases, as well as a source of fluorescence signaling.

Ghosh and Saha investigated the tris-amine-coupled benzimidazolium-based tricationic fluorescent chemosensor **175** (Fig. 22), which has high selectivity towards $H_2PO_4^-$.[126] $H_2PO_4^-$ in CH_3CN promotes anion-induced quenching of the emission of **175** along with the formation of a weak excimer peak at 500 nm. The monomer emission of **175** decreases during titration with $H_2PO_4^-$, followed by an increase in the excimer emission of **175** with an isosbestic point at 487 nm. Receptor **175** showed selectivity towards sensing of ATP over ADP and AMP in aqueous CH_3CN ($CH_3CN:H_2O$ = 3 : 2 v/v) by exhibiting an increase in emission. The stoichiometry of the ATP complex with **175** was 2 : 1 (guest : host). Electrostatic charge–charge interactions along with both conventional (N–H···X; X═O, halides) and unconventional (C^+–H···X; X═O, halides) hydrogen bonding between the host and the guest molecule were synergistically involved in causing complex formation.

Schäferling and co-workers reported a water-soluble polythiophene derivative **176** (Fig. 22) as a probe for colorimetric and fluorescence sensing of ATP in a buffered aqueous solution.[127] The fluorescence of **176** at 520 nm is quenched by ATP if the concentration of Mg^{2+} is lower than 0.5 mmol L^{-1}. Upon addition of ATP, the conformation of **176** changes to a helix, as seen by the formation of strong CD peaks. Furthermore, the guanosine phosphates GTP, GDP and GMP generate similar spectral responses to the corresponding adenosine phosphates. However, the guanine unit causes an additional fluorescence quenching effect, presumably by a photoinduced charge transfer process. These observations revealed that two factors contribute to the fluorescence response, one being structural changes of the polymer backbone induced by interactions with the triphosphate units, and the other fluorescence quenching produced by the single nucleobase units.

Lysosomes in astrocytes and microglia release ATP as a cell signaling molecule in response to various stimuli through Ca^{2+}-dependent exocytosis. Wang's group synthesized a series of derivatives **177** (Fig. 22) that can be specifically localized in lysosomes where they serve as fluorescent probes to sense ATP in cells.[128] These probes exhibited high selectivity and sensitivity for ATP at physiological pH values with a detection limit as low as 10^{-11} M. Probe **177** has high selectivity, appreciable photostability and good biocompatibility in living cells. It can also be applied to fluorescence microscopy based real-time monitoring of changes in concentrations of ATP in lysosomes.

Zhu and co-workers reported amphiphilic imidazolium derivative **178** bearing a cetyl chain as an ATP selective fluorescent probe, in which a dansyl group both serves as a fluorescent source and recognizes the adenine base *via* π–π interactions (Fig. 22).[129] On the other hand, imidazolium and sulfonamide moieties can recognize ATP *via* either hydrogen bonding interactions or electrostatic interactions. Finally, cetyl groups enable the formation of self-assembled micelles. The critical micellar concentration (CMC) was calculated to be 7.67 μM. At pH 7.4 (PBS buffer, 1 mM), probe **178** displayed weak yellow emission at 535 nm, which was blue-shifted to show green emission at 508 nm upon the addition of ATP. Among various anions such as F^-, Cl^-, Br^-, AcO^-, CO_3^{2-}, NO_3^-, Pi, PPi, AMP, ADP, UDP, UTP and ATP, only ATP induced a highly selective fluorescence change, which was attributed to the interaction of imidazolium $(CH)^+$ and amide NH hydrogens with ATP. This system was further applied to monitor the activity of apyrase, which can convert ATP to ADP, AMP and Pi. ATP imaging in HepG-2 liver cancer cells was also successfully demonstrated using this system.

Li and co-workers also described a facile colorimetric method for ATP sensing based on ATP-induced aggregation of Au@**179** NPs incorporating bis-imidazolium groups.[130] Fig. 23 illustrates the sensing mechanism of **179** for colorimetric detection of ATP. Complexation of **179** with ATP causes AuNP aggregation, which promotes a red-shift in the characteristic LSPR band because of the strong plasmon coupling between neighboring nanoparticles. This is accompanied by a color change from red to blue that can be observed by the naked eye. Triphosphate was more effective than di- or mono-phosphate groups in promoting aggregate formation. As a result, **179** can easily distinguish ATP (1 μM to 1 mM) from ADP (20 μM) and AMP (500 μM). Changing the ATP concentration promotes changes in the extent of aggregation of the AuNPs. As a result, this system can be used to monitor ATP concentrations. The lowest detection concentration of ATP was 0.1 μM.

4.1.2 GTP sensing. Kim and co-workers showed that the imidazolium-anthracene cyclophane **180** (Fig. 24) can be used to differentiate structurally similar GTP and ATP, and it displays incredibly high selectivity for I^- among halides and other anions (*e.g.* NO_3^- and HSO_4^-).[131] This fluorescent chemosensor, containing four imidazolium units, is a cyclophane derivative that serves the dual function of a halide and nucleotide sensor in 100% aqueous solution through chelation-enhanced fluorescence quenching (CHEQ) of excimer emission. Notably,

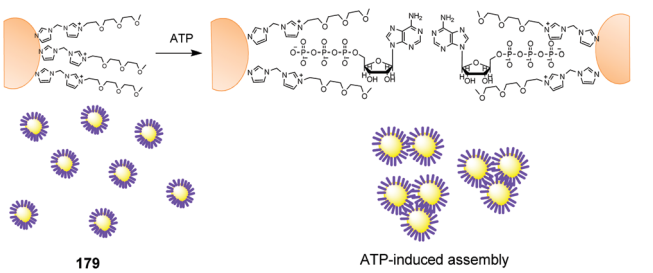

Fig. 23 Schematic illustration of the sensing mechanism of ATP-induced assembly of Au@**179** nanoparticles.

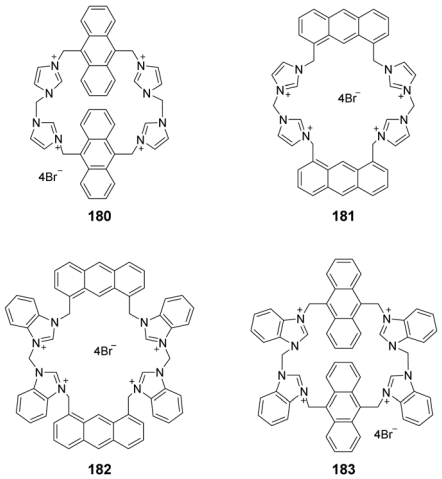

Fig. 24 Structure of compounds **180–183**.

the fluorescence of **180** is ''turned off'' upon addition of GTP and changes to green in the presence of 1-ATP. The color change is presumably due to the 25 nm blue-shift in the excimer emission. Furthermore, significant CHEQ in both monomer and excimer emission is exhibited by **180**–I^-, which can be attributed to a heavy atom effect. The detection limits of **180** for GTP and I^- are 4.8×10^{-7} and 8×10^{-5} M, respectively.

Kim and co-workers also reported the results of studies with the derivative **181** (Fig. 24), which enables differentiation of the structurally similar GTP and ATP in 100% aqueous solutions (pH = 7.4, 10 mM phosphate buffer).[132] This fluorescent chemosensor detects GTP by a chelation-enhanced fluorescence quenching (CHEQ) effect with the formation of excimer emission at 490 nm. In contrast, ATP promotes the chelation-enhanced fluorescence (CHEF) of **181**. The binding constant of **181** with GTP was determined to be 1×10^6 M^{-1}, while that with ATP was 7.4×10^5 M^{-1}. The detection limits of this sensor were 9.7×10^{-7} M and 1.4×10^{-6} M for GTP and ATP, respectively. These large affinities can be attributed to strong $(C–H)^+\cdots A^-$ ionic H-bonding.

Kim and co-workers designed cyclophanes **182** and **183** and demonstrated that these benzimidazolium based substances (Fig. 24) are ideal candidates for highly selective sensing of GTP and I^- in 100% aqueous solutions.[133] The fluorescence was quenched by the addition of GTP, due to the π–H interactions with the base in addition to the $(C–H)^+\cdots A^-$ ionic hydrogen-bonding interactions with I^- among nucleotides in 100% aqueous solutions (pH = 7.4).

You and co-workers developed the imidazolium-functionalized squaraine **184** (Fig. 25) as a sensitive colorimetric and fluorescent chemosensor for GTP in aqueous solutions.[134] An observable color change occurs from azure to navy blue upon addition of GTP to a buffered solution of **184**. Other anions including ATP, PPi, GDP, GMP, phosphate, halide, acetate, bicarbonate, sulfate and nitrate do not cause this effect. With increasing amounts of GTP, the absorption of monomeric **184** at approximately 658 nm was weakened significantly, and the absorption of the aggregates at approximately 557 nm is enhanced gradually, with a detection

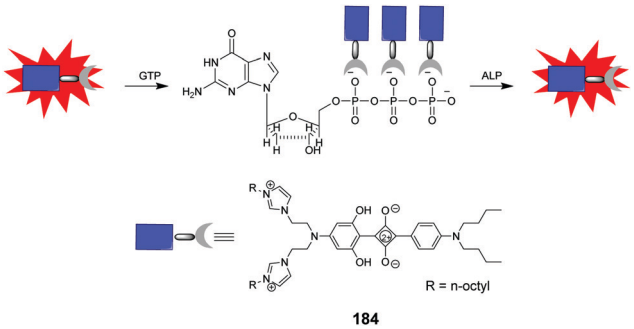

Fig. 25 The proposed model of the host–guest interaction between **184** and GTP.

limit for GTP up to 5.4 ppb. Squaraine **184** exhibits good water-solubility, but it is also capable of entering the cells as an imaging reagent. Hydrolysis of GTP to form GDP, GMP, guanosine and phosphate catalyzed by alkaline phosphatase (ALP) induces fluorescence turn-on, which means that **184** can be applied in enzyme activity assays. Fig. 25 shows the proposed model of the host–guest interaction between **184** and GTP.

4.1.3 DNA sensing. Kim and co-workers described anthracene derivative **185** (Fig. 26) in which two imidazolium groups are present at the 1- and 8-positions of the anthracene ring in the absence of a linker.[5] In aqueous solutions, **185** exhibited selective fluorescence quenching promoted only by DNA and not various other nucleotide anions. The association constant of the complex formed between **185** and DNA was calculated to be 8.9×10^6 M^{-1}. Furthermore, hydrolysis of CTDNA with DNase in the presence of Mg^{2+} can be monitored using fluorescent probe **185**. Specifically, because ct-DNA effectively quenches the fluorescence of **185**, hydrolysis by DNase induces a ''turn-on'' signal.

Human DNA has various types of secondary structures, such as B-DNA, Z-DNA and hairpins. Guanine rich sequences, like

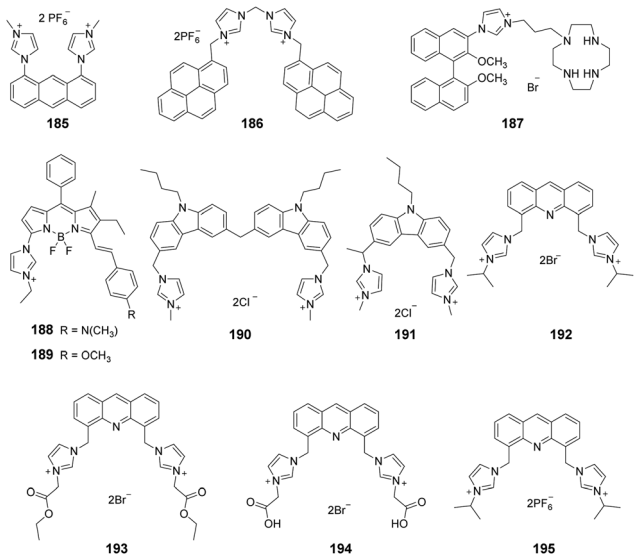

Fig. 26 Structure of compounds **185–195**.

those in G-quadruplexes formed from four stranded guanine bases and stabilized by monovalent cations, play an important role in cancer cell growth and the control of gene expression in telomeres. Yoon and co-workers reported that pyrene-imidazolium derivative **186** (Fig. 26) can selectivity recognize G-quadruplexes using fluorescence and NMR spectroscopy.[4] It was observed that the ratio of excimer and monomer emission of the pyrene fluorophore in **186** changes when the sensor binds to GGG sequences on the groove of the G-quartet. This interaction induced an excimer emission enhancement of **186** at 482 nm. The binding constant for the complex was calculated to be 5.5×10^5 M^{-1}. In contrast to other sensors that recognize the preformed G-quartet DNA structure, **186** is thought to be a ''G-quartet inducer'' in which it interacts with the G-rich DNA region to initiate production of the G-quartet structure. Also, the groove binding characteristic of **186** to the G-quadruplex resulted in only relatively low non-specific toxicity, and the structure-specific differences in the fluorescence characteristics between the DNA duplex and G-quadruplex may offer an avenue to discover applications of this probe in biological studies.

Yu and co-workers developed the water-soluble imidazolium-based BINOL receptor **187** (Fig. 26), which selectively senses DNA over other biologically relevant anions including nucleotides under physiological conditions.[135] A non-covalent, intercalation and/or groove binding mode of this receptor takes place with DNA that is driven by the propensity of DNA to bind small molecules *via* hydrophobic, π-stacking, electrostatic and/or hydrogen bonding interactions. Free **187** displayed a broad emission band with a maximum at 451 nm and a large Stokes shift (160 nm, quantum yield 0.021). Upon addition of 2 equiv. ct-DNA, the emission maximum undergoes a blue-shift to 412 nm together with an intensity enhancement (quantum yield 0.025). The association constant between **187** and DNA was $4.4 \pm 1 \times 10^4$ M^{-1}.

Cao and co-workers developed two BODIPY-imidazolium salts, **188** and **189** (Fig. 26), as sensitive and selective fluorescent intercalators for DNA.[136] The observation of strong hypochromism and a red-shifted absorption band of **188**, together with the marked decrease in the positive CD band of ct-DNA, is consistent with the occurrence of strong intercalation of the probe with DNA. The fluorescence of **188** differs somewhat from that of **189**. Addition of ct-DNA to a solution containing **188** elicited a dramatic increase in the 586 nm emission along with a large fluorescence enhancement. A substantial enhancement of the fluorescence intensity around 609 nm occurred in **189**. The binding constants for DNA were 4.5×10^3 and 1.9×10^3 for **188** and **189**, respectively. Furthermore, the existence of intercalative interactions in these binding events was supported by the results of time-resolved fluorescence studies. The excited-state lifetimes of **189** and **189** became longer when both were complexed with DNA. The decay time of **188** in the presence ct-DNA was 2.7 ns, and that for **189** was approximately 3.7 ns.

Bao and co-workers described the methylene bridged cationic biscarbazole derivative **190** (Fig. 26) and investigated its spectroscopic properties and its binding abilities with both DNA and nucleotides.[137] To gain a better understanding of this probe, its monomeric analogue **191** was also synthesized and investigated. The binary carbazole **190** exhibited higher binding abilities with both ct-DNA and nucleotides than its monomeric counterpart **191**. The respective calculated Hypo% values were 38.80% for **190** (calculated in the region of [DNA]/[23] $\geq$ 1.0) and 13.20% for **191** at 10 mM ionic strength, and 32.40% and 14.10% at 50 mM ionic strength. Thus, **190** exhibited a higher hypochromic effect than **191**, which indicated that it has a higher DNA binding ability. The results of spectral investigations suggested that the higher ability of the binary carbazole **190** to bind both ct-DNA and nucleotides than its monomeric form was a consequence of the structurally flexible nature of the non-rigid methylene-linked bis-carbazole.

Prabusankar and co-workers synthesized a series of water soluble acridine derivatives **192–195** (Fig. 26) consisting of imidazolium salts with alkyl, ester and carboxylic acid functional groups.[138] The acridine derivative of an imidazolium salt with a bromide counter anion, **192**, existed in a different molecular orientation compared to the analogous imidazolium salt **195** containing a hexafluorophosphate counter anion. The fluorescence of these compounds was quenched upon addition of ct-DNA, suggesting that the probes bind to DNA. However, analysis of fluorescence quenching data showed that the binding constant of **192** (28.1×10^6 M^{-1}) was much higher than those of **193–195** (9.1×10^6 M^{-1} for **193**; 2.7×10^6 M^{-1} for **194**; and 10.1×10^6 M^{-1} for **195**), suggesting that **192** has a comparatively higher affinity for ct-DNA. CD spectra of DNA are usually altered upon binding of ligands such as small organic or drug molecules due to induced conformational changes. Addition of **192**, **193** or **194** resulted in changes in the magnitudes of the negative and positive CD ellipticity peaks at 245 nm or 275 nm.

Li and co-workers described the bifunctional perylene-tetracarboxylic acid di-imide (PDI) **196** (Fig. 27) containing non-covalently modified graphene groups.[139] This molecule consisted of a core of five connected benzene rings and two positive side arms in which the core plays a role in π–π interactions with graphene, and each arm acts as a bridge to enable grafting of gold nanoparticles (AuNPs). The Au–PDI–graphene nanohybrid was designed to be a label-free electrochemical impedance hairpin DNA (hpDNA) biosensor for

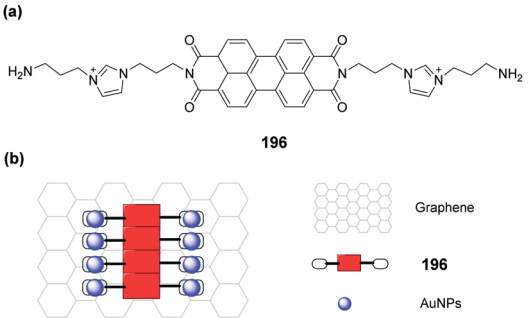

Fig. 27 (a) Structures of molecule Au–**196**–graphene. (b) Schematic representation of Au–**196**–graphene nanohybrid fabrication and hpDNA hybridization detection.

detection of human immunodeficiency virus 1 gene. The fabricated hpDNA biosensor was found to display a relatively low detection limit (1.2×10^{-15} M). This nanohybrid strategy has the potential of being applied to the design of probes for a broad range of possible DNA sequences as part of specific applications in biodiagnostics and bionanotechnology.

4.1.4 RNA sensing. The water-soluble imidazolium naphthalene derivative **197** (Fig. 28), which is a specific turn-on fluorescent sensor for RNA in 100% aqueous solution (pH = 7.4, 10 mM phosphate buffer), was reported by Kim's group.[6] Only minor changes (quenching) occur upon addition of 1 equiv. of sodium salts of the phosphate anions of ATP, GTP, CTP, UTP, TTP, pyrophosphate (PPi)) and DNA to **197**. On the other hand, turn-on fluorescence occurred at 449 nm when this probe was treated with RNA, which was apparent in the form of a blue color enhancement. The binding constant of **197** with RNA was determined to be 4.9×10^6 M^{-1}. This large affinity is attributed to the presence of strong complementary $(C–H)^+ \cdots A^-$ ionic H-bonding with the phosphate group of RNA and π-stacking of the aromatic part of cyclophane **197** with RNA. Furthermore, fluorescence image detection of RNA in living cells such as onion cells, HeLa cells, and animal model cells was successfully carried out with **197**, which displayed a chelation-enhanced fluorescence effect.

Nam and co-workers also reported the results of studies with the tetra-cationic probe **198** (Fig. 28), whose fluorescence is selectively enhanced upon addition of RNA.[140] As a membrane permeable fluorescent probe, **198** can be used for selective imaging of RNA both in the human neuroblastoma tumor SH-SY5Y cell line used for Parkinson's disease and in unicellular green alga cells.

A concise and explicit binding mechanism for fluorescence sensing of RNA is essential for further development of fluorescent molecules that have high selectivity and specificity towards RNA. Kim and co-workers noted that the principle of neighbor-exclusion is violated in RNA by a series of naphthalene-based cationic probes **199–203** (Fig. 28).[141] In contrast to insertion in DNA, only the naphthalene moiety is small enough to be inserted into intercalation sites of RNA compared to pyrene and anthracene. Moreover, both specific bases (but all stacking pairs) are responsible for fluorescence changes through π–π interactions with the probes. The results of molecular dynamics (MD) simulations indicated the existence of stable intercalation structures with these probes in which the imidazolium moieties interact with two H-bonding acceptors (the negatively charged oxygen of phosphate and the 2′-OH of ribose) both present in RNA. This provides selectivity for binding RNA as compared to DNA, which only has a phosphate backbone and lacks the ribose 2′-OH. The computational results support the CD experimental results, which suggest that RNA is stretched upon intercalation of the probe molecules. Furthermore, breaking of the spatial overlap between the HOMO and LUMO in the excited states of the probes leads to charge transfer driven de-excitation corresponding to fluorescence at 425–450 nm. Overall, the small fluorophore of the naphthalene group needed for facile intercalation (and at least one cationic moiety for hydrogen bonding) along with their straightforward synthesis makes these probes useful for studying RNA recognition.

4.2 Other anions

Xu and co-workers reported three imidazolium derivatives **204–206** in which the naphthaimidazolium group acted as both a fluorophore and anion receptor (Fig. 29).[142] Compound **204** exhibited high selectivity for F^- in a CH_3CN solution over all the other anions and acts as a ratiometric fluorescent probe for F^- with an enhanced blue-shift in emission. However, the fluorescence of **205** and **206**, which was quenched and blue-shifted in the presence of fluoride ions, can be quenched by other tested anions, where the degree of quenching depends on the characteristic of the anions. More importantly, only **204** can be utilized to ratiometrically detect F^- in a DMSO–water (95 : 5, v/v) aqueous solution. It was deduced that **204** is bound to F^- mainly by the force of hydrogen bonding, while **205** and **206** coordinate with F^- through electrostatic interactions.

Jang and co-workers reported receptor **207**, which contains a benzothiazole group conjugated with an imidazolium cation.[143] This sensor is capable of selectively binding Hg(II) in the presence of other metal ions in water. This binding resulted in a large enhancement in the fluorescence intensity at 380 nm because it prevented PET quenching (Fig. 30). An analysis of the F_{450}/F_{380} plot and interference studies showed that the Hg(II) complex of receptor **207** is useful for selective analysis of Br^- ions in water, even when other anions are present. The probe has a Hg(II) detection limit of 22 nM. The results of ^1H NMR

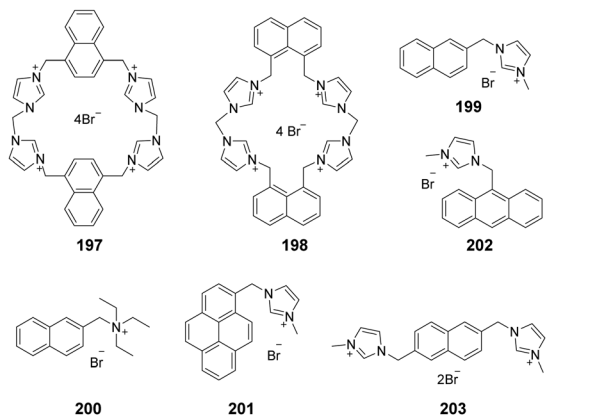

Fig. 28 Structure of compounds **197–203**.

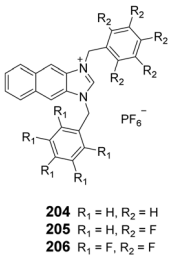

Fig. 29 Structure of compounds **204–206**.

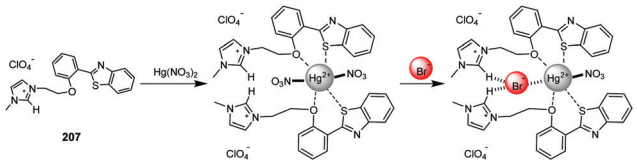

Fig. 30 Plausible binding modes of **207** with Hg(II) and Br^- ions.

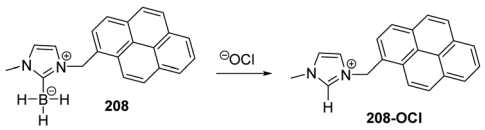

Fig. 31 Reaction mechanism of probe **208** with OCl^-.

studies showed that the imidazolium hydrogen in the Hg(II) complex with receptor **207** participates in the recognition of Br^- ions. In the absence of Hg(II), receptor **207** does not respond to Br^- ions.

Yoon and co-workers reported a pyrene derivative **208** bearing N-heterocyclic carbene (NHC) boranes as a OCl^- selective probe at pH 7.4 (10 mM PBS containing 1% CH_3CN).[144] Among various ROS including H_2O_2 and $ONOO^-$, OCl^- selectively reduces the excimer emission at 477 nm, and the monomeric emission at 374 nm was increased as shown in Fig. 31. Arylboronic acids were reported as ROS selective probes *via* a nucleophilic oxidation mechanism. In contrast, probe **208** bearing NHC boranes reacted with OCl^- to afford its corresponding imidazolium product *via* the electrophilic oxidation mechanism. This unique and selective conversion can control the extent of excimer formation. Aggregated excimer formation is preferred due to the low polarity of probe **208**. TPM was successfully applied to image HOCl ratiometrically both in living cells and tissues. 710 nm was used for excitation, and blue emission (380–420 nm) and green emission (480–600 nm) were observed. When exogeneous NaOCl was introduced into the RAW 264.7 macrophages, F_{green}/F_{blue} changed from 5.13 to 2.50. Similar results were obtained when RAW 264.7 cells were incubated with lipopolysaccharides (LPS) followed by interferons (IFN-γ). Myeloperoxidase (MPO) is known to convert H_2O_2 to $HOCl/OCl^-$. Only a slight decrease of F_{green}/F_{blue} was observed upon the addition of MPO inhibitors, such as 4-aminobenzoic acid hydrazide (4-ABAH) and flufenamic acid (FAA).

Sessler and co-workers synthesized eight fluorescent polymeric gels to prepare a two-layer gel for chloride anion recognition.[145] The fluorescent groups contained either coumarin, BODIPY, or rhodamine. Gels **209–212** containing calix[4] pyrrole (C4P)/imidazolium-F-anion recognition motifs were used to construct a fluorescent pattern (Code A) for the robust bottom layer. Gels **213–216** based on C4P/imidazolium–Br^- anion interactions were used to construct an array (Code B) for the top layer (Fig. 32a). The double layer code system, in which Code B adhered to the surface of Code A, was stabilized by interfacial C4P/imidazolium–Br^- anion interactions (Fig. 32b). In the double code system, only the encoded information of the top layer (Code B) could be read

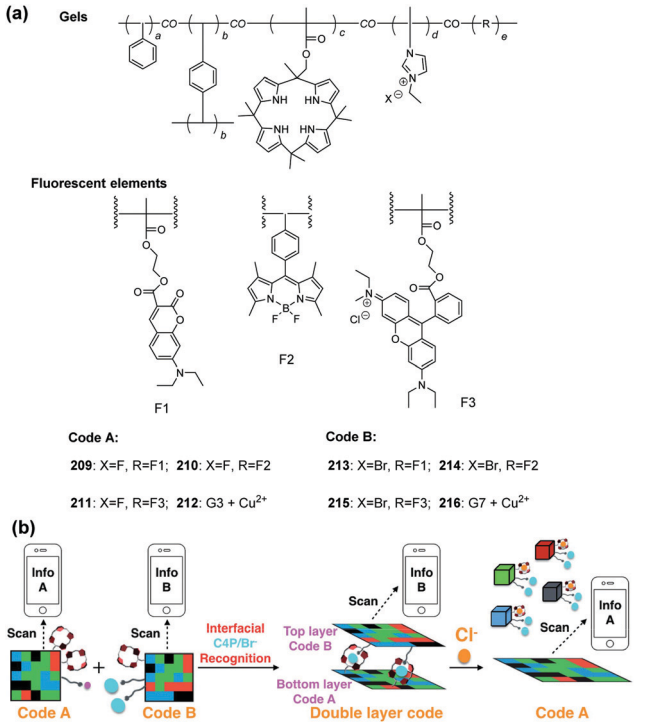

Fig. 32 (a) Chemical structures of the polymeric gels, the incorporated fluorescent elements, and the recognition elements present in Code A (**209–212**) and Code B (**213–216**). (b) The mechanism of forming a double layer code and specific sensing of Cl^- anions.

out. The addition of Cl^- anions could separate the two layers and read out Code A by delaminating the top layer and leaving the bottom layer intact. This sensing strategy allowed direct recognition of the chloride anion using a smart phone.

Kumar and co-workers developed a 1-(40-nitrophenyl)benzimidazolium based chemodosimeter **217** (Fig. 33), which displayed an instantaneous (<60 s) ratiometric fluorescence signal in response to up to 1 equiv. of cyanide ions in 95% HEPES buffer (5% DMSO).[146] Also, **217** undergoes a ~20-fold

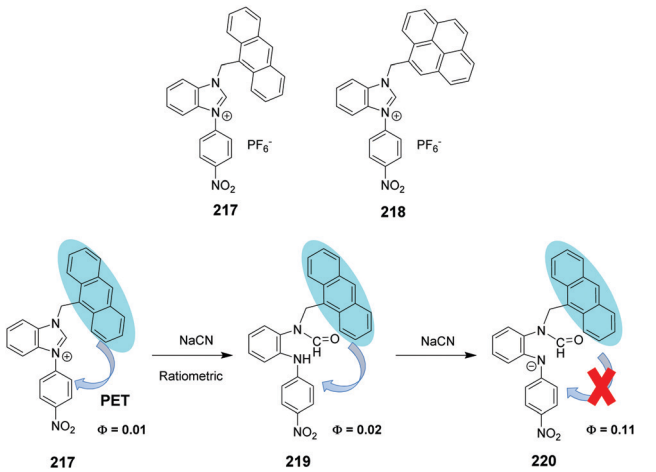

Fig. 33 Structure of compounds **217–220**, and the proposed mechanism of **217** for cyanide detection.

fluorescence intensity increase in response to changes in the amount of cyanide ions present between 1 and 5 equiv. (Fig. 29). X-ray crystal structure analysis and the results of photophysical and theoretical studies confirmed the following mechanism: PET is replaced by exciplex formation through conversion to a formamide derivative **219**, and the exciplex was broken due to the formation of anion **220** by further reaction with cyanide. Chemodosimeter **217** can be used for highly selective and ratiometric detection of cyanide with a detection limit of 30 nM. The probe also can be used to measure cyanide ions in the presence of human blood serum. Chemodosimeter **218**, which contains a pyrene fluorophore, also displays a selective response to cyanide in HEPES buffer (5% DMSO). However, this probe cannot be used for ratiometric measurement of cyanide ions using fluorescence.

Chae and co-workers reported three binary ensemble systems consisting of an imidazolium-bearing dansyl-based probe **221** and three dicynovinyl group-containing substrates with different alkyl chain lengths to detect CN^- in a buffer solution of HEPES : DMSO (2 : 8) (pH = 7.4) (Fig. 34).[147] These ensembles gave strong emission at 525 nm due to the dansyl group positioned in the hydrophobic interior and showed selective "turn on" fluorescence emission upon addition of CN^-. The association constants of the three ensemble systems with CN^- were calculated to be **221**–S1 ($2.38 \times 10^8\ M^{-1}$) > **221**–S2 ($7.52 \times 10^7\ M^{-1}$) > **221**–S3 ($1.17 \times 10^7\ M^{-1}$). This result indicated the importance of the alkyl chain length for highly sensitive CN^- detection. The limits of detection were determined to be 200 nM, 1 μM and 2 μM, respectively.

Masson and co-workers synthesized two hydrophobic 1-(carboxyalkyl)-3-(12-mercaptododecyl)-1*H*-imidazolium ionic liquids with different counterions (Br^-, BF_4^-, PF_6^-, ClO_4^-, and NTf_2^-) and alkyl chain lengths (ethyl and pentyl) to form monolayers and reduce the nonspecific adsorption of a concentrated cell lysate (Fig. 35).[148] $[(HS)^{12}C_{12}(COOH)^2C_2im]^+Br^-$ **222** was the most efficient ionic liquid monolayer, and the surface coverage of **222** was as low as 2 ± 2 ng cm^{-2}. The ionic liquid monolayer of $[(HS)^{12}C_{12}(COOH)^5C_5im]^+Br^-$ **223** was modified with anti-HER2 and was used successfully to detect HER2 from a crude breast cancer cell lysate.

Zhou and co-workers designed a novel multi-ion-responsive probe **224**, imidazolium chloride ionic liquid-grafted rhodamine B salicyl aldehyde hydrazone, which can individually identify Cu^{2+} and Al^{3+} in 100% aqueous solutions (Fig. 35).[149] **224** displayed a significant color change from colorless to pink

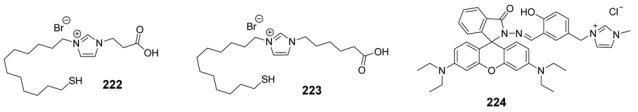

Fig. 35 Structure of compounds **222–224**.

upon addition of Cu^{2+} and Al^{3+} accompanied by a large increase at 561 nm in absorbance, which was due to the spirolactam ring-opening. More importantly, **224** can effectively discriminate between Cu^{2+} and Al^{3+} depending on the electrostatic repulsion-induced difference in response times (less than 1 min for Cu^{2+} and more than 5 h for Al^{3+}).

Wei and co-workers synthesized imidazolium ionic liquid-functionalized silicon nanoparticles (**225**@SiNP) which were highly sensitive and selective towards Hg^{2+} ions through a label-free method (Fig. 36).[150] Hg^{2+} showed stronger affinity to imidazolium groups on the surface of **225**@SiNP than that of other metal ions. Thus, Hg^{2+} induced the fluorescence quenching of **225**@SiNP up to 70%. The mechanism was verified by dynamic quenching UV-vis absorption spectroscopy and fluorescence lifetime experiments. A good linear relationship was obtained in the range of 0–40 μM with a detection limit of 0.45 μM for Hg^{2+} detection. Furthermore, the amphiphilicity of **225**@SiNP can easily be changed through anion exchange without multiple surface modifications.

Cell surface carbohydrates can differ considerably in diseased *versus* healthy organisms. As a result, unique glycan markers can be exploited for early disease diagnosis, and the development of vaccines and therapeutics. Galan and co-workers developed an imidazolium tagged-mannosamine derivative (ITag-Man) for the non-covalent, rapid and site-specific labelling of sialic acid containing glycoproteins in a range of cell lines.[151] The general strategy for the use of ITag-sugars as non-covalent probes in metabolic oligosaccharide engineering (MOE) is shown in Fig. 37a. ITag-mannosamine (Ac4ManN-ITag, **226**) was synthesized for non-covalent labeling of glycoconjugates in live cells. The labelling process, using commercially available *N*-nitrilotriacetate fluorescent reagent NTA-Atto 550, is mild and fast, and it is bioorthogonal and complimentary to current labelling methods. The corresponding neuraminic acid derivative **227** was used for deacetylating **226** by treatment with D-sialic acid aldolase in the presence of pyruvate, demonstrating that **226** is tolerated by an aldolase. The ITags are well tolerated by a number of cell lines including Jurkat T-lymphocytes, breast cancer cell line MDA-MB-231 (MDA), colon cancer cell line HT29-MTX-E12 (E12),

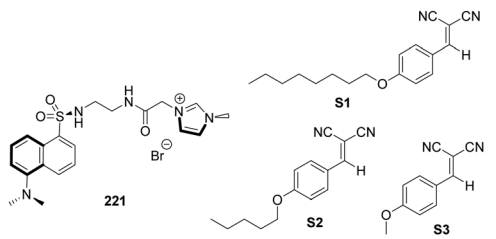

Fig. 34 Structures of imidazolium-bearing dansyl-based probe **221** and the benzylidenemalononitrile substrates (**S1**, **S2** and **S3**).

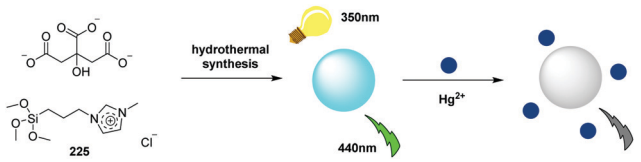

Fig. 36 Schematic illustration of the preparation process of **225**@SiNP nanoparticles and their application for Hg^{2+} detection.

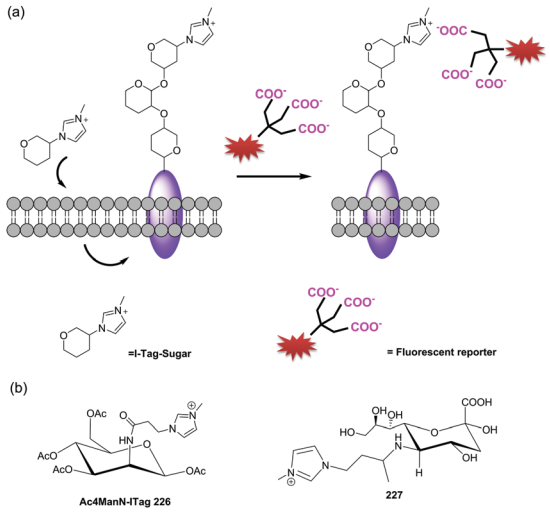

Fig. 37 (a) General strategy for the use of ITag-sugars as non-covalent probes in MOE. (b) Structure of Ac4ManN-ITag **226** and neuraminic acid derivative **227**.

cervical cancer cells, HeLa and SV40-immortalized human corneal epithelium (AS) cells. Moreover, this reagent does not have a significant effect on cell adhesion or the overall magnitude of cell surface charge. In addition, a chelating affinity column was used to enrich the sample with glycoproteins specifically labelled with the new ITag-sialic acid moieties.

5. Conclusions

Studies of imidazolium salts as anion receptors began nearly 20 years ago.[152–154] Due to the fact that the imidazolium group is able to bind anions in aqueous solution, its derivatives with diverse topological features have been widely used for sensing various anions. In the past six years, new and important contributions have been made in the development of imidazolium receptors, such as the use of a combination of imidazolium and halogen-bonding,[25–28] an expansion of imidazolium conjugated systems[9–19] and the creation of new scaffolds.[21–23,29–31] Some imidazolium-derived fluorescent probes have been applied to sensing phosphate-containing anions,[124–141] such as ATP, GTP, DNA and RNA. We hope that this review, which summarizes the progress made over the past years, will enable scientists working in this area to focus their future studies on the conjugation of imidazolium with biomolecules and fluorophores, as well as on methods to improve the feasibility of applications of imidazolium in biological samples.

Conflicts of interest

There are no conflicts to declare.

Acknowledgements

This study was supported by grants from the National Research Foundation of Korea (NRF) funded by the Korean government (MSIP) (No. 2012R1A3A2048814 for J. Y.). Z. X. thanks the National Natural Science Foundation of China (22078314, 21878286). Y. H. thanks the National Natural Science Foundation of China (21807093).

Notes and references

1 M. J. Langton, C. J. Serpell and P. D. Beer, *Angew. Chem., Int. Ed.*, 2016, **55**, 1974–1987.
2 J. Yoon, S. K. Kim, N. J. Singh and K. S. Kim, *Chem. Soc. Rev.*, 2006, **35**, 355–360.
3 Z. Xu, S. K. Kim and J. Yoon, *Chem. Soc. Rev.*, 2010, **39**, 1457–1466.
4 H. N. Kim, E. H. Lee, Z. Xu, H. E. Kim, H. S. Lee, J. H. Lee and J. Yoon, *Biomaterials*, 2012, **33**, 2282–2288.
5 H. N. Kim, J. Lim, H. N. Lee, J. W. Ryu, M. J. Kim, J. Lee, D. U. Lee, Y. Kim, S. J. Kim and K. D. Lee, *Org. Lett.*, 2011, **13**, 1314–1317.
6 B. Shirinfar, N. Ahmed, Y. S. Park, G. S. Cho, I. S. Youn, J. K. Han, H. G. Nam and K. S. Kim, *J. Am. Chem. Soc.*, 2013, **135**, 90–93.
7 Z. Xu, N. J. Singh, J. Lim, J. Pan, H. N. Kim, S. Park, K. S. Kim and J. Yoon, *J. Am. Chem. Soc.*, 2009, **131**, 15528–15533.
8 Z. Xu, N. R. Song, J. H. Moon, J. Y. Lee and J. Yoon, *Org. Biomol. Chem.*, 2011, **9**, 8340–8345.
9 Z. Xu, S. K. Kim, S. J. Han, C. Lee, G. Kociok-Kohn, T. D. James and J. Yoon, *Eur. J. Org. Chem.*, 2009, 3058–3065.
10 A. K. Mahapatra, G. Hazra and P. Sahoo, *Bioorg. Med. Chem. Lett.*, 2012, **22**, 1358–1364.
11 N. R. Song, J. H. Moon, J. Choi, E. J. Jun, Y. Kim, S. J. Kim, J. Y. Lee and J. Yoon, *Chem. Sci.*, 2013, **4**, 1765–1771.
12 M. Grzybowski, E. Glodkowska-Mrowka, V. Hugues, W. Brutkowski, M. Blanchard-Desce and D. T. Gryko, *Chem. – Eur. J.*, 2015, **21**, 9101–9110.
13 J.-F. Lefebvre, D. Leclercq, J. P. Gisselbrecht and S. Richeter, *Eur. J. Org. Chem.*, 2010, 1912–1920.
14 Q. Xu, C. H. Heo, G. Kim, H. W. Lee, H. M. Kim and J. Yoon, *Angew. Chem., Int. Ed.*, 2015, **54**, 4890–4894.
15 Z. Guo, N. R. Song, J. H. Moon, M. Kim, E. J. Jun, J. Choi, J. Y. Lee, C. W. Bielawski, J. L. Sessler and J. Yoon, *J. Am. Chem. Soc.*, 2012, **134**, 17846–17849.
16 S. H. Mashraqui, R. Betkar, M. Chandiramani, D. Quinonero and A. Frontera, *Tetrahedron Lett.*, 2010, **51**, 596–599.
17 C. Gao, G. Gao, J. Lan and J. You, *Chem. Commun.*, 2014, **50**, 5623–5625.
18 J. T. Hutt, J. Jo, A. Olasz, C. H. Chen, D. Lee and Z. D. Aron, *Org. Lett.*, 2012, **14**, 3162–3165.
19 Y. Yang, F. Qiu, C. Xu, Y. Feng, G. Zhang and W. Liu, *Dalton Trans.*, 2018, **47**, 7480–7486.
20 G. T. Spence, C. J. Serpell, J. Sardinha, P. J. Costa, V. Félix and P. D. Beer, *Chem. – Eur. J.*, 2011, **17**, 12955–12966.
21 P. Sabater, F. Zapata, A. Caballero, I. Fernandez, C. Ramirez de Arellano and P. Molina, *J. Org. Chem.*, 2016, **81**, 3790–3798.

22 S. Kumari, S. Joshi, T. C. Cordova-Sintjago, D. D. Pant and R. Sakhuja, *Sens. Actuators, B*, 2016, **229**, 599–608.
23 S. Chaudhary and M. D. Milton, *J. Photochem. Photobiol., A*, 2018, **356**, 595–602.
24 G. R. Desiraju, P. S. Ho, L. Kloo, A. C. Legon, R. Marquardt, P. Metrangolo, P. Politzer, G. Resnati and K. Rissanen, *Pure Appl. Chem.*, 2013, **85**, 1711–1713.
25 A. Caballero, N. G. White and P. D. Beer, *Angew. Chem., Int. Ed.*, 2011, **50**, 1845–1848.
26 F. Zapata, A. Caballero, N. G. White, T. D. Claridge, P. J. Costa, V. Felix and P. D. Beer, *J. Am. Chem. Soc.*, 2012, **134**, 11533–11541.
27 M. Cametti, K. Raatikainen, P. Metrangolo, T. Pilati, G. Terraneo and G. Resnati, *Org. Biomol. Chem.*, 2012, **10**, 1329–1333.
28 P. Sabater, F. Zapata, A. Caballero, N. de la Visitacion, I. Alkorta, J. Elguero and P. Molina, *J. Org. Chem.*, 2016, **81**, 7448–7458.
29 M. Feng, X. Jiang, Z. Dong, D. Zhang, B. Wang and G. Gao, *Tetrahedron Lett.*, 2012, **53**, 6292–6296.
30 D. Zhang, H. Yang, A. Martinez, K. Jamieson, J. P. Dutasta and G. Gao, *Chem. – Eur. J.*, 2014, **20**, 17161–17167.
31 T. S. Pandian, V. Srinivasadesikan, M. C. Lin and J. Kang, *Tetrahedron*, 2015, **71**, 7782–7788.
32 R. Kumar, S. Kumar, P. Singh, G. Hundal, M. S. Hundal and S. Kumar, *Analyst*, 2012, **137**, 4913–4916.
33 E. J. Jun, H. Liu, J. Y. Choi, J. Y. Lee and J. Yoon, *Sens. Actuators, B*, 2013, **176**, 611–617.
34 A. Kumar and H. S. Kim, *New J. Chem.*, 2015, **39**, 2935–2942.
35 A. Kumar, A. Pandith and H. S. Kim, *Dyes Pigm.*, 2015, **122**, 351–358.
36 M. W. Ahmad, S. H. Kim and H. S. Kim, *Tetrahedron Lett.*, 2011, **52**, 6743–6747.
37 Z. Xu, J. Y. Choi and J. Y. Yoon, *Bull. Korean Chem. Soc.*, 2011, **32**, 1371–1374.
38 L. Ding, Y. Bai, Y. Cao, G. Ren, G. J. Blanchard and Y. Fang, *Langmuir*, 2014, **30**, 7645–7653.
39 S. Long, Q. Qiao, F. Deng, L. Miao, J. Yoon and Z. Xu, *Chem. Commun.*, 2019, **55**, 969–972.
40 S. Long, Q. Qiao, L. Miao and Z. Xu, *Chin. Chem. Lett.*, 2019, **30**, 573–576.
41 S. Long, L. Miao, R. Li, F. Deng, Q. Qiao, X. Liu, A. Yan and Z. Xu, *ACS Sens.*, 2019, **4**, 281–285.
42 H. Taoa, L. Hea, G. Cheng and Q. Y. Cao, *Dyes Pigm.*, 2019, **166**, 233–238.
43 C. Li, Y. Xu, J. Yang, Y. Chen, H. S. Kim, Q. Cao and J. S. Kim, *Sens. Actuators, B*, 2017, **251**, 617–623.
44 W. Gong, S. Wang, Y. Wei, L. Ding and Y. Fang, *Spectrochim. Acta, Part A*, 2017, **170**, 198–205.
45 H. Seema, B. Shirinfar, G. Shi, S. Youn and N. Ahmed, *J. Phys. Chem. B*, 2017, **121**, 5007–5016.
46 Y. Zhang, J. Cao and L. Ding, *J. Photochem. Photobiol., A*, 2017, **333**, 56–62.
47 K. Chen and M. Schmittel, *Chem. Commun.*, 2014, **50**, 5756–5759.
48 W. Zhang, S. Y. Gan, F. H. Li, D. X. Han, Q. X. Zhang and L. Niu, *RSC Adv.*, 2015, **5**, 2207–2212.
49 S. Marullo, F. D'Anna, M. Cascino and R. Noto, *J. Org. Chem.*, 2013, **78**, 10203–10208.
50 H. Liu, L. Zhang, J. Chen, Y. Zhai, Y. Zeng and L. Li, *Anal. Bioanal. Chem.*, 2013, **405**, 9563–9570.
51 W. Wang, A. Fu, J. Lan, G. Gao, J. You and L. Chen, *Chem. – Eur. J.*, 2010, **16**, 5129–5137.
52 L. González-Mendoza, B. Altava, M. I. Burguete, J. Escorihuela, E. Hernando, S. V. Luis, R. Quesada and C. Vicent, *RSC Adv.*, 2015, **5**, 34415–34423.
53 L. Gonzalez-Mendoza, J. Escorihuela, B. Altava, M. I. Burguete and S. V. Luis, *Org. Biomol. Chem.*, 2015, **13**, 5450–5459.
54 F. Zapata, S. J. Benítez-Benítez, P. Sabater, A. Caballero and P. Molina, *Molecules*, 2017, **22**, 2273.
55 P. Sabater, F. Zapata, A. Caballero, N. Visitación, I. Alkorta, J. Elguero and P. Molina, *J. Org. Chem.*, 2016, **81**, 7448–7458.
56 Q. Liu, X. Zhao, Z. Hu, Z. Zhao and H. Wang, *Sci. Rep.*, 2017, **7**, 7534.
57 Y. Liu, Z. Zhao and Q. Liu, *Sci. Rep.*, 2018, **8**, 10943.
58 S. Kumar, P. Singh and S. Kumar, *Tetrahedron Lett.*, 2012, **53**, 2248–2252.
59 E. J. Jun, Z. Xu, M. Lee and J. Yoon, *Tetrahedron Lett.*, 2013, **54**, 2755–2758.
60 K. Ghosh, D. Kar and P. R. Chowdhury, *Tetrahedron Lett.*, 2011, **52**, 5098–5103.
61 K. Ghosh, D. Kar, D. Sahu and B. Ganguly, *RSC Adv.*, 2015, **5**, 46608–46616.
62 K. Ghosh, S. S. Ali and S. Joardar, *Tetrahedron Lett.*, 2012, **53**, 2054–2058.
63 F. Zapata, P. Sabater, A. Caballero and P. Molina, *Org. Biomol. Chem.*, 2015, **13**, 1339–1346.
64 T. S. Pandian, V. Srinivasadesikan, M. C. Lin and J. Kang, *Tetrahedron*, 2015, **71**, 8350–8356.
65 D. Zhang, X. Jiang, Z. Dong, H. Yang, A. Martinez and G. Gao, *Tetrahedron*, 2013, **69**, 10457–10462.
66 D. Lee, C. Lee, E. J. Jun, M. Lee, S. Park and J. Yoon, *ChemistryOpen*, 2017, **6**, 476–479.
67 H. Zhang, X. Shao, C. Chipot and W. Cai, *J. Phys. Chem. C*, 2019, **123**, 11304–11309.
68 D. Kong, T. Weng, W. He, B. Liu, S. Jin, X. Hao and S. Liu, *J. Organomet. Chem.*, 2013, **727**, 19–27.
69 J. B. Zhuo, C. Y. Zhang, C. X. Lin, S. Bai, L. L. Xie and Y. F. Yuan, *J. Organomet. Chem.*, 2014, **763–764**, 34–43.
70 J. B. Zhuo, C. X. Lin, Q. Wan, L. L. Xie and Y. F. Yuan, *J. Organomet. Chem.*, 2015, **791**, 289–297.
71 J. Cao, L. Ding, W. Hu, X. Chen, X. Chen and Y. Fang, *Langmuir*, 2014, **30**, 15364–15372.
72 J. Y. Jung, E. J. Jun, Y. U. Kwon and J. Yoon, *Chem. Commun.*, 2012, **48**, 7928–7930.
73 M. Lee, J. H. Moon, E. J. Jun, G. Kim, Y. U. Kwon, J. Y. Lee and J. Yoon, *Chem. Commun.*, 2014, **50**, 5851–5853.
74 S. Kumar, S. Arora, P. Singh and S. Kumar, *RSC Adv.*, 2012, **2**, 9969–9975.

75 B. Roy, A. K. Bar, B. Gole and P. S. Mukherjee, *J. Org. Chem.*, 2013, **78**, 1306–1310.
76 D. H. Wang, Z. Gong, R. Sun and D. Z. Zhao, *New J. Chem.*, 2015, **39**, 5991–5996.
77 A. Singh, A. Singh, N. Singh and D. O. Jang, *RSC Adv.*, 2015, **5**, 72084–72089.
78 J. B. Czirok, M. Bojtár, D. Hessz, P. Baranyai, L. Drahos, M. Kubinyi and I. Bitter, *Sens. Actuators, B*, 2013, **182**, 280–287.
79 Y. Yao, K. Jie, Y. Zhou and M. Xue, *Tetrahedron Lett.*, 2014, **55**, 3195–3199.
80 Y. Yang, X. Wang, Q. Cui, Q. Cao and L. Li, *ACS Appl. Mater. Interfaces*, 2016, **8**, 7440–7448.
81 G. A. Marceloa, S. M. G. Piresb, M. A. F. Faustinob, M. M. Q. Simõesb, M. G. P. M. S. Nevesb, H. M. Santosa, J. L. Capeloa, J. P. Motad, C. Lodeiroa and E. Oliveira, *Dyes Pigm.*, 2019, **161**, 427–437.
82 Q. Kong, W. Zhuang, G. Li, Q. Jiang and Y. Wang, *New J. Chem.*, 2018, **42**, 9187–9192.
83 L. Yang, S. Qin, X. Su, F. Yang, J. You, C. Hu, R. Xie and J. Lan, *Org. Biomol. Chem.*, 2010, **8**, 339–348.
84 Q. S. Lu, J. Zhang, L. Jiang, J. T. Hou and X. Q. Yu, *Tetrahedron Lett.*, 2010, **51**, 4395–4399.
85 Q. Lu, J. Hou, J. Wang, B. Xu, J. Zhang and X. Yu, *Chin. J. Chem.*, 2013, **31**, 641–650.
86 K. Swamy, N. J. Singh, J. Yoo, S. K. Kwon, S. Y. Chung, C. H. Lee and J. Yoon, *J. Inclusion Phenom. Macrocyclic Chem.*, 2010, **66**, 107–111.
87 F. Song, N. Fei, F. Li, S. Zhang, Y. Cheng and C. Zhu, *Chem. Commun.*, 2013, **49**, 2891–2893.
88 E. Faggi, R. Porcar, M. Bolte, S. V. Luis, E. Garcia-Verdugo and I. Alfonso, *J. Org. Chem.*, 2014, **79**, 9141–9149.
89 A. Caballero, N. G. White and P. D. Beer, *CrystEngComm*, 2014, **16**, 3694–3698.
90 N. Mesquida, I. Dinares, A. Ibanez and E. Alcalde, *Org. Biomol. Chem.*, 2013, **11**, 6385–6396.
91 P. Sabater, F. Zapata, A. Caballero, I. Alkorta, C. R. Arellano, J. Elguero and P. Molina, *ChemistrySelect*, 2018, **3**, 3855–3859.
92 J. Yang, C. C. Dong, X. L. Chen, X. Sun, J. Y. Wei, J. F. Xiang, J. L. Sessler and H. Y. Gong, *J. Am. Chem. Soc.*, 2019, **141**, 4597–4612.
93 J. Zhou, Y. Yuan, J. Zhuo and C. Lin, *Tetrahedron Lett.*, 2018, **59**, 1059–1064.
94 V. Suresh, N. Ahmed, I. S. Youn and K. S. Kim, *Chem. – Asian J.*, 2012, **7**, 658–663.
95 M. Yousuf, N. Ahmed, B. Shirinfar, V. M. Miriyala, I. S. Youn and K. S. Kim, *Org. Lett.*, 2014, **16**, 2150–2153.
96 Y. Chun, N. J. Singh, I. C. Hwang, J. W. Lee, S. U. Yu and K. S. Kim, *Nat. Commun.*, 2013, **4**, 1797–1804.
97 D. Zhang, X. Jiang, H. Yang, Z. Su, E. Gao, A. Martinez and G. Gao, *Chem. Commun.*, 2013, **49**, 6149–6151.
98 H. Y. Gong, B. M. Rambo, V. M. Lynch, K. M. Keller and J. L. Sessler, *Chem. – Eur. J.*, 2012, **18**, 7803–7809.
99 H. Y. Gong, B. M. Rambo, V. M. Lynch, K. M. Keller and J. L. Sessler, *J. Am. Chem. Soc.*, 2013, **135**, 6330–6337.
100 J. Shang, B. M. Rambo, X. Hao, J.-F. Xiang, H.-Y. Gong and J. L. Sessler, *Chem. Sci.*, 2016, **7**, 4148–4157.
101 M. Toure, L. Charles, C. Chendo, S. Viel, O. Chuzel and J. L. Parrain, *Chem. – Eur. J.*, 2016, **22**, 8937–8942.
102 C. J. Serpell, J. Cookson, A. L. Thompson and P. D. Beer, *Chem. Sci.*, 2011, **2**, 494–500.
103 H. Zhou, Y. Zhao, G. Gao, S. Li, J. Lan and J. You, *J. Am. Chem. Soc.*, 2013, **135**, 14908–14911.
104 J.-H. Wang, J.-B. Xiong, X. Zhang, S. Song, Z.-H. Zhu and Y.-S. Zheng, *RSC Adv.*, 2015, **5**, 60096–60100.
105 J. R. Jadhav, C. H. Bae and H.-S. Kim, *Tetrahedron Lett.*, 2011, **52**, 1623–1627.
106 J. R. Jadhav, M. W. Ahmad and H. S. Kim, *Bull. Korean Chem. Soc.*, 2011, **32**, 2933–2937.
107 A. Tripathi and P. S. Pandey, *Tetrahedron Lett.*, 2011, **52**, 3558–3560.
108 Q. Liu, H. Wu, Z. Zhao and D. Wei, *Tetrahedron*, 2019, **75**, 3128–3134.
109 Z. Xu, N. Singh, S. K. Kim, D. R. Spring, K. S. Kim and J. Yoon, *Chem. – Eur. J.*, 2011, **17**, 1163–1170.
110 V. Amendola, M. Boiocchi, L. Fabbrizzi and N. Fusco, *Eur. J. Org. Chem.*, 2011, 6434–6444.
111 X. Chen, S. Kang, M. J. Kim, J. Kim, Y. S. Kim, H. Kim, B. Chi, S. J. Kim, J. Y. Lee and J. Yoon, *Angew. Chem., Int. Ed.*, 2010, **49**, 1422–1425.
112 X. Chen, K.-M. Lee and J.-Y. Yoon, *Bull. Korean Chem. Soc.*, 2011, **32**, 3775–3778.
113 Q. Xu, S. Lee, Y. Cho, M. H. Kim, J. Bouffard and J. Yoon, *J. Am. Chem. Soc.*, 2013, **135**, 17751–17754.
114 S. Lee, H. Cheng, M. Chi, Q. Xu, X. Chen, C. Y. Eom, T. D. James, S. Park and J. Yoon, *Biosens. Bioelectron.*, 2016, **77**, 1016–1019.
115 Z. Zhang, J. Li, F. Wang, T. Wei, Y. Chen, J. Qiang, T. Xiao and X. Chen, *Sens. Actuators, B*, 2019, **282**, 636–643.
116 Y. Huang, H. C. Pappas, L. Zhang, S. Wang, R. Cai, W. Tan, S. Wang, D. G. Whitten and K. S. Schanze, *Chem. Mater.*, 2017, **29**, 6389–6395.
117 H. Qi, L. Zhang, L. Yang, P. Yu and L. Mao, *Anal. Chem.*, 2013, **85**, 3439–3445.
118 S. Hussain, A. H. Malik and P. K. Iyer, *ACS Appl. Mater. Interfaces*, 2015, **7**, 3189–3198.
119 N. Zehra, D. Dutta, A. H. Malik, S. S. Ghosh and P. K. Iyer, *ACS Appl. Mater. Interfaces*, 2018, **10**, 27603–27611.
120 Q. Cui, X. Wang, Y. Yang, S. Li, L. Li and S. Wang, *Chem. Mater.*, 2016, **28**, 4661–4669.
121 C. C. Hua, Q. Gao, S. Liu, L. L. Chang, K. S. Xia, B. Han and C. G. Zhou, *Chem. Eng. J.*, 2018, **346**, 458–465.
122 X. Wang, Y. Wang, X. Ye, T. Wu, H. Deng, P. Wu and C. Li, *Biosens. Bioelectron.*, 2018, **99**, 34–39.
123 X. Sun, Y. Qian, Y. Jiao, J. Liu, F. Xi and X. Dong, *Talanta*, 2017, **165**, 429–435.
124 D. Wang, X. Zhang, C. He and C. Duan, *Org. Biomol. Chem.*, 2010, **8**, 2923–2925.
125 H. N. Kim, J. H. Moon, S. K. Kim, J. Y. Kwon, Y. J. Jang, J. Y. Lee and J. Yoon, *J. Org. Chem.*, 2011, **76**, 3805–3811.
126 K. Ghosh and I. Saha, *Supramol. Chem.*, 2011, **23**, 518–526.

127 C. Spangler, T. Lang and M. Schferling, *Dyes Pigm.*, 2012, **95**, 194–200.
128 B. H. Huang, Z. R. Geng, X. Y. Ma, C. Zhang, Z. Y. Zhang and Z. L. Wang, *Biosens. Bioelectron.*, 2016, **83**, 213–220.
129 J. H. Zhu, C. Yu, Y. Chen, J. Shin, Q.-Y. Cao and J. S. Kim, *Chem. Commun.*, 2017, **53**, 4342–4345.
130 Y. Yang, Q. Cui, Q. Cao and L. Li, *Colloids Surf., A*, 2016, **503**, 28–33.
131 N. Ahmed, B. Shirinfar, I. Geronimo and K. S. Kim, *Org. Lett.*, 2011, **13**, 5476–5479.
132 N. Ahmed, B. Shirinfar, I. S. Youn, A. Bist, V. Suresh and K. S. Kim, *Chem. Commun.*, 2012, **48**, 2662–2664.
133 N. Ahmed, B. Shirinfar, I. S. Youn, M. Yousuf and K. S. Kim, *Org. Biomol. Chem.*, 2013, **11**, 6407–6413.
134 N. Wu, J. Lan, L. Yan and J. You, *Chem. Commun.*, 2014, **50**, 4438–4441.
135 M.-Q. Wang, K. Li, H. R. Xu and X. Q. Yu, *Anal. Methods*, 2013, **5**, 5903–5907.
136 C. Zhao, Y. Zhang, X. Wang and J. Cao, *J. Photochem. Photobiol., A*, 2013, **264**, 41–47.
137 G. Li, X. Zhou, P. Yang, Y. Jian, T. Deng, H. Shen and Y. Bao, *Tetrahedron Lett.*, 2014, **55**, 7054–7059.
138 G. Raju, S. Vishwanath, A. Prasad, B. K. Patel and G. Prabusankar, *J. Mol. Struct.*, 2016, **1107**, 291–299.
139 W. Zhang, F. Li, Y. Hu, S. Gan, D. Han, Q. Zhang and L. Niu, *J. Mater. Chem. B*, 2014, **2**, 3142–3148.
140 N. Ahmed, B. Shirinfar, V. M. Miriyala, S.-K. Choi, K.-M. Lee, W. B. Jeon, Y. S. Park and H. G. Nam, *Supramol. Chem.*, 2014, **27**, 478–483.
141 M. Yousuf, I. S. Youn, J. Yun, L. Rasheed, R. Valero, G. Shi and K. S. Kim, *Chem. Sci.*, 2016, **7**, 3581–3588.
142 C. Zou, Q. Qiao, M. Zhao, D. Mao, D. Wang, L. Feng, J. Cui and Z. Xu, *RSC Adv.*, 2014, **4**, 43746–43751.
143 A. Singh, A. Singh, N. Singh and D. O. Jang, *Tetrahedron Lett.*, 2016, **72**, 3535–3541.
144 Y. L. Pak, S. J. Park, D. Wu, B. H. Cheon, H. M. Kim, J. Bouffard and J. Yoon, *Angew. Chem., Int. Ed.*, 2018, **57**, 1567–1571.
145 X. Ji, W. Chen, L. Long, F. Huang and J. L. Sessler, *Chem. Sci.*, 2018, **9**, 7746–7752.
146 S. Kumar, P. Singh, G. Hundal, M. S. Hundal and S. Kumar, *Chem. Commun.*, 2013, **49**, 2667–2669.
147 E. Jeong, S. Yoon, H. S. Lee, A. Kumara and P. S. Chae, *Dyes Pigm.*, 2019, **162**, 348–357.
148 A. Aubé, S. Campbell, A. R. Schmitzer and J. F. Masson, *Analyst*, 2017, **142**, 2343–2353.
149 C. C. Hua, Q. Gao, Z. X. Zhu, L. L. Chang, K. S. Xia, B. Han and C. G. Zhou, *Sens. Actuators, B*, 2018, **259**, 411–419.
150 Q. Li, K. Peng, Y. Lu, A. Li, F. Che, Y. Liu, X. Xi, Q. Chu, T. Lan and Y. Wei, *J. Mater. Chem. B*, 2018, **6**, 8214–8220.
151 D. Benito-Alifonso, S. Tremell, J. C. Sadler, M. Berry and M. C. Galan, *Chem. Commun.*, 2016, **52**, 4906–4909.
152 K. Sato, S. Arai and T. Yamagishi, *Tetrahedron Lett.*, 1999, **40**, 5219–5222.
153 E. Alcalde, N. Mesquida, L. Pérez-García, C. Alvarez-Rúa, S. García-Granda and E. García-Rodriguez, *Chem. Commun.*, 1999, 295–296.
154 H. Ihm, S. Yun, H. G. Kim, J. K. Kim and K. S. Kim, *Org. Lett.*, 2002, **4**, 2897–2900.

